Basin Research (1996) **8**, 329–349

Predicting sediment flux from fold and thrust belts

Gregory E. Tucker* and Rudy Slingerland

Department of Geosciences and Earth System Science Center, Pennsylvania State University, USA

ABSTRACT

The rate of sediment influx to a basin exerts a first-order control on stratal architecture. Despite its importance, however, little is known about how sediment flux varies as a function of morphotectonic processes in the source terrain, such as fold and thrust growth, variations in bedrock lithology, drainage pattern changes and temporary sediment storage in intermontane basins. In this study, these factors are explored with a mathematical model of topographic evolution which couples fluvial erosion with fold and thrust kinematics. The model is calibrated by comparing predicted topographic relief with relief measured from a DEM of the Central Zagros Mountains fold belt. The sediment-flux curve produced by the Zagros fold belt simulation shows a delay between the onset of uplift and the ensuing sediment flux response. This delay is a combination of the natural response time of the geomorphic system and a time lag associated with filling, and then subsequently uplifting and re-eroding, the proximal part of the basin. Because deformation typically propagates toward the foreland, the latter time lag may be common to many ancient foreland basins. Model results further suggest that the response time of the bedrock fluvial system is a function of rock resistance, of the width of the region subject to uplift and erosion, and, assuming a nonlinear dependence of fluvial erosion upon channel gradient, of uplift rate. The geomorphic response time for the calibrated Zagros model is on the order of a few million years, which is commensurate with, or somewhat larger than, typical recurrence intervals for episodes of thrusting. However, model experiments also highlight the potential for significant variations in both geomorphic response time and in sediment flux as a function of varying rock resistance. Given a reasonable erodibility contrast between resistant and erodible lithologies, model sediment flux curves show significant sediment flux variations that are related solely to changes in rock resistance as the outcrop pattern changes. An additional control on sediment flux to a basin is drainage diversion in response to folding or thrusting, which can produce major shifts in the location and magnitude of sediment source points. Finally, these models illustrate the potential for a significant mismatch between tectonic events and sediment influx to a basin in cases where sediment is temporarily ponded in an intermontane basin and later remobilized.

INTRODUCTION

The least well studied control on stratal architecture in sedimentary basins is the rate of sediment influx. While numerous studies have documented the roles of sea level (e.g. Kendall & Lerche, 1988; Posamentier *et al.*, 1988; Cant, 1989; Posamentier & Allen, 1993a,b) and subsidence (e.g. Jordan & Flemings, 1991; Devlin *et al.*, 1993; Steckler *et al.*, 1993; Williams & Dobb, 1993; Cant & Stockmal, 1994) in producing stratigraphic sequences, most researchers, for want of more information, have considered sediment flux as a knob to be turned at will. Only recently has the role of sediment flux been examined in any detail (Christie-Blick, 1991; Slingerland & Zhang, 1991; Jervey, 1992; Heller *et al.*, 1993; Schlager, 1993; Slingerland *et al.*, 1993; Steckler *et al.*, 1993), and numerous questions remain. What is the functional relationship between the volume of sediment delivered to a basin and such independent variables in the source terrain as relief and climate? To what extent are variations in sediment influx produced by morphotectonic processes in the source terrain, such as (1) the episodic growth and geomorphic decay of individual structures, (2) exposure of lithologies of varying resistance to erosion, (3) changes in drainage basin size and geometry (for example by stream capture) and (4) temporary sediment storage in

*Now at: Ralph M. Parsons Laboratory, Department of Civil and Environmental Engineering, Massachusetts Institute of Technology, Cambridge, MA 02139, USA.

© 1996 Blackwell Science Ltd

intermontane basins? And more generally, what is the shape of a sediment yield curve through time in response to a period of deformation in a typical fold and thrust belt? Only by answering these questions can we properly interpret the sedimentary record contained in foreland basins.

Here we use a mathematical model of landscape evolution to investigate the roles of fold growth, lithological variations and drainage network rearrangement in moderating the sediment influx to a foreland basin from a fold and thrust belt. As a case study, we consider the Zagros Mountains of south-western Iran, a young and presently active fold and thrust belt. The Zagros are an especially interesting case because they are quite young (~5 Ma; Berberian & King, 1981) and because erosion has unroofed a relatively uniform (laterally) succession of marine to paralic strata. These two characteristics allow a fairly straightforward tectonic and stratigraphic reconstruction. By combining a fluvial erosion model with tectonic reconstructions of fold development in the Zagros, and by calibrating the resulting model based on the modern topographic relief of the orogen, it is possible to examine the time-evolving geomorphic and sedimentary response to foreland fold development. In addition, this paper also considers the more general case of a foreland subject to intermittent thrusting.

LANDSCAPE EVOLUTION MODEL

The model employed in this study is a variant of GOLEM (Tucker & Slingerland, 1994; Tucker, 1996), a landscape evolution model that computes the passage of water and sediment across a planform finite-difference grid (Fig. 1). The elevation of each grid cell represents the elevation of a primary stream channel embedded within the cell (in the manner of Howard *et al.*, 1994), and the drainage area for each point on the grid is computed using a steepest-descent flow accumulation algorithm (Tucker & Slingerland, 1994). Channel discharge is modelled as the integral of the precipitation rate over the upstream contributing area at each point. Because precipitation is herein assumed to be uniform in space, this implies that

$$Q = PA \tag{1}$$

where Q is a long-term effective channel discharge, P is precipitation rate and A is upstream drainage area.

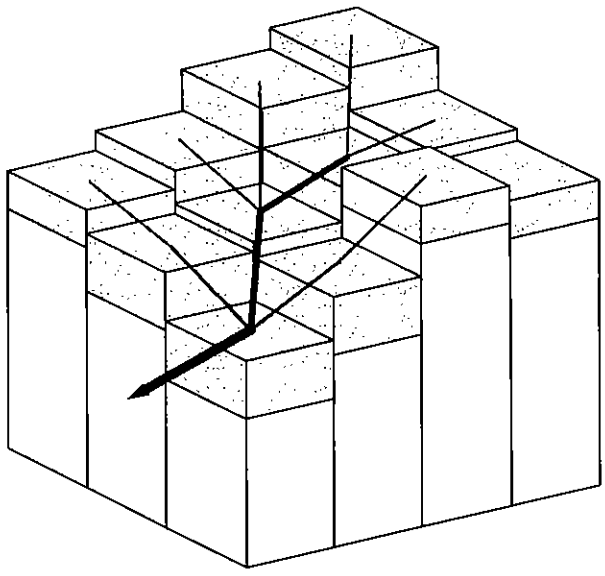

Fig. 1. Model representation of topography and drainage. Each model cell has dimensions Δx by Δx and consists of one or more lithologies capped by a variably thick sediment cover.

Bedrock channels

Two types of fluvial channel may occur in the model: bedrock channels and alluvial channels (Howard, 1980, 1987). The former are assumed to occur wherever a stream's capacity to entrain and transport particles exceeds the locally available sediment supply. The latter occur where the converse is true. Bedrock channels can be expected to be the dominant channel type in mountainous topography. The incision rate of bedrock channels is here modelled as a power function of channel gradient, S, and discharge, Q, according to

$$\frac{\partial h_b}{\partial t} = -k_b Q^m S^n \tag{2}$$

where t is time and h_b represents the elevation of the channel bed relative to a datum within the underlying rock column that moves up or down according to the rate of tectonic uplift or subsidence, $U(x, y, t)$ (Howard *et al.*, 1994). There are only a handful of studies that bear on the choice of parameters k_b, m and n; these are reviewed by Howard *et al.* (1994) and will be only briefly summarized here.

In a study of bedrock streams in the Oregon Coast Ranges, Seidl & Dietrich (1992) demonstrated that the product of channel gradient and drainage area at tributary junctions is roughly the same for tributaries and trunk streams. If one assumes that long-term effective channel discharge varies linearly with drainage area, this implies that

$$\frac{m}{n} \cong 1. \tag{3}$$

This finding is consistent with the hypothesis that channel incision rate varies as a function of stream power, or the discharge–slope product with $m = n = 1$ (Seidl & Dietrich, 1992; Seidl *et al.*, 1994). Alternatively, based on studies of bedrock channel incision in badlands, Howard & Kerby (1983) and Howard (1994) suggested that in some cases the channel incision rate may vary in proportion to bed shear stress, τ, according to

$$\frac{\partial h_b}{\partial t} = -k_r \tau \tag{4}$$

where k_r is a proportionality constant that reflects the

© 1996 Blackwell Science Ltd,

efficiency of channel erosion for a given shear stress. Bed shear stress can be related to channel gradient and discharge by considering the following relationships:

$$\tau = \rho g R S \quad \text{steady, uniform flow} \tag{5}$$

$$R \cong d \quad \text{wide channels} \tag{6}$$

$$Q = VWd \quad \text{continuity of mass} \tag{7}$$

$$V = \sqrt{\frac{8gRS}{f}} \quad \text{D'Arcy–Weisbach equation} \tag{8}$$

where ρ is water density, g is gravitational acceleration, R is hydraulic radius, d is channel depth, W is channel width, V is mean flow velocity and f is a dimensionless friction factor (Yalin, 1977). Combining Eqs (5)–(8) gives

$$\tau = \frac{\rho g^{2/3} f^{1/3}}{2}\left(\frac{Q}{W}\right)^{2/3} S^{2/3}. \tag{9}$$

The width of natural channels commonly varies as a function of discharge according to

$$W = k_w Q^{m_w} \tag{10}$$

where k_w and m_w are constants, and m_w is typically $\cong 0.5$ (Yalin, 1992). Combining Eqs (4), (9) and (10), and assuming $m_w = 0.5$, we have

$$\frac{\partial h_b}{\partial t} = -k_b Q^{1/3} S^{2/3} \tag{11}$$

and

$$k_b = k_t\left(\frac{\rho g^{2/3} f^{1/3}}{2k_w^{2/3}}\right). \tag{12}$$

Model calibration studies based on topographic relief and slope–area relationships in the Central Zagros (Tucker, 1996) suggest that the exponents in Eq. (11) are more appropriate than the stream power exponents of Eq. (3) for this region, and therefore Eq. (11) is adopted in this study.

In order to rationalize the dimensions of the constant k_b in Eq. (11), the equation can be reformulated in terms of an 'erosional velocity', k_v, and a characteristic channel discharge, Q_*, as

$$\frac{\partial h_b}{\partial t} = -k_v\left(\frac{Q}{Q_*}\right)^m S^n. \tag{13}$$

For the purposes of this study, Q_* represents the maximum potential channel discharge, equal to the total area of the model grid times the assumed precipitated rate; the values of m and n are 1/3 and 2/3, respectively, as derived above.

Alluvial channels

Alluvial channels are assumed to occur wherever the local sediment supply equals or exceeds the transport capacity. In fold and thrust belts like the Zagros, such channels are most common in intermontane basins where a decrease in channel gradient leads to aggradation. Treatment of sediment transport capacity in the model is based on the Bagnold (1966) bed-load transport formula, as modified by Bridge & Dominic (1984):

$$Q_s = \frac{Wa_t}{(\sigma - \rho)\rho^{1/2} g}(\tau - \tau_c)(\tau^{1/2} - \tau_c^{1/2}) \tag{14}$$

where Q_s is the volumetric total bed load transport rate, τ is bed shear stress, τ_c is the critical shear stress for entrainment of sediment particles, g is gravitational acceleration, σ is sediment bulk density, W is channel width and a_t is a dimensionless constant. If $\tau \gg \tau_c$, this reduces to

$$Q_s = \frac{a_t W}{(\sigma - \rho)\rho^{1/2} g}\tau^{3/2}. \tag{15}$$

Substituting Eq. (10) for W and Eq. (9) for τ, we find that

$$Q_s = k_f Q S \tag{16}$$

where

$$k_f = \frac{a_t \rho f^{1/2}}{2(\sigma - \rho)}. \tag{17}$$

Of these, only f varies appreciably along a channel; for simplicity, it is held constant here. For alluvial channels, continuity of mass implies that the rate of change of channel elevation, in the absence of tectonic uplift or subsidence, is proportional to downstream changes in the discharge–slope product:

$$\frac{\partial h_b}{\partial t} = -\frac{k_f}{W}\frac{\partial QS}{\partial \bar{x}} \tag{18}$$

where $\bar{x}$ denotes distance along a channel.

Hillslope processes

The rate at which sediment is delivered to a channel network from hillslopes and first-order channels is largely a function of processes that operate on too fine a scale to be explicitly treated at the scale of interest in this study. In regions of high relief, and particularly in arid settings like the Zagros Mountains, slope transport is often dominated by mass-wasting processes such as debris flows and landsliding. In such settings, slopes are typically maintained at or near a threshold failure angle (Carson & Pelty, 1970; Carson & Kirkby, 1972; Moon & Selby, 1983), and therefore respond very rapidly to changes in base level along a trunk stream. These characteristics allow for the simple assumption that the average elevation of hillsides within a 1-km² grid cell moves up or down through time at the same rate as the channel that is explicitly modelled.

Channel transitions

In the model, a transition from a bedrock channel to an alluvial channel will occur wherever the total available

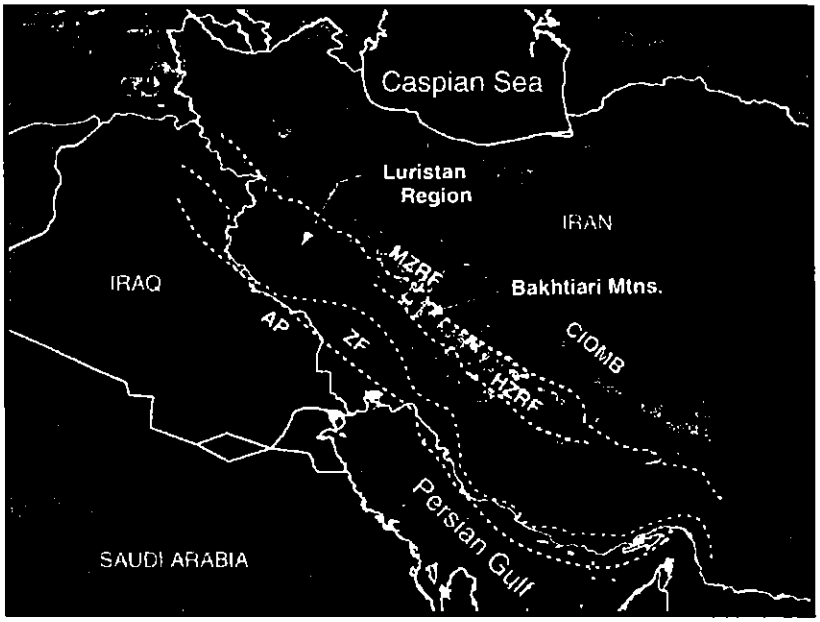

Fig. 2. Shaded relief image of topography in the Zagros and adjoining regions. MZRF: Main Zagros reverse fault; HZRF: High Zagros reverse fault; ZF: inner Zagros foreland basin; AP: Arabian platform and outer foreland basin; CIOMB; Central Iranian ophiolite–melange belts. Topography is from ETOPO5 5-arc-minute global elevation data set published by the National Geophysical Data Center. Tectonic zones are from Berberian & King (1981).

sediment supply (defined as the supply from upstream plus any locally stored sediment) equals or exceeds the transport capacity, which is given by Eq. (16). Conversely, a transition from an alluvial channel to a bedrock channel will occur wherever the total sediment supply drops below the stream's carrying capacity, for instance where a stream exits a piggyback basin and crosses an emergent fold or thrust. The interaction between these two channel types gives rise to a third transitional category, analogous to the 'mixed bedrock–alluvial' category defined by Howard *et al.* (1994). This third channel type occurs where a stream is only slightly below its carrying capacity, so that the amount of incision is limited to that amount which produces just enough sediment to satisfy the carrying capacity. Another way to say this is that the channel gradient cannot drop below the minimum gradient required to transport the imposed sediment supply. In terms of longitudinal profile evolution, these mixed bedrock–alluvial channels in the model behave in exactly the same manner as alluvial channels, because in both cases the sediment transport rate is the limiting variable.

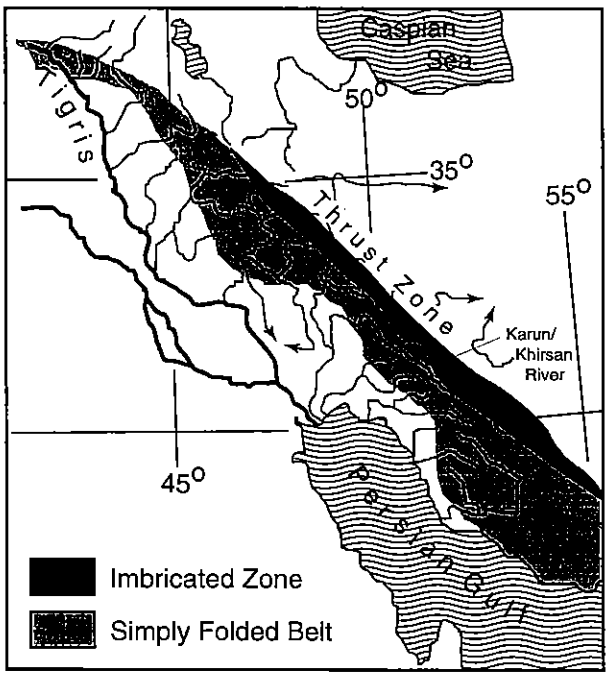

Fig. 3. Structural zones and transverse drainage of the Zagros Mountains. Modified from Oberlander (1965) and Falcon (1974).

INITIAL AND BOUNDARY CONDITIONS

In order to keep the model experiments grounded in a real geological example, the initial and boundary conditions are based on the tectonics of the Zagros Mountains fold and thrust belt. The Zagros Mountains are part of the Alpine–Himalayan orogenic system (Fig. 2). The orogen can be divided into three structural zones: an inner crystalline zone of overthrusting, an imbricated belt and a zone of folding often referred to as the Simply Folded Belt (Falcon, 1969) (Fig. 3). The inner portion of the orogen has been subject to intermittent deformation extending at least as far back as the late Palaeozoic (Berberian & King, 1981). By contrast, the modern fold and thrust belt (comprising the imbricate zone and the Simply Folded Belt) was a relatively quiescent region of sediment accumulation until the latest episode of shortening and uplift began in the late Miocene or early Pliocene (James & Wynd, 1965; Falcon, 1974; Berberian & King, 1981). Stratigraphic and geomorphic evidence indicates that deformation has propagated from north-east to south-west through time (Oberlander, 1965; Falcon, 1974; Berberian & King, 1981; Mann & Vita-Finzi, 1988) and continues to the present day. The exact timing of the onset of the most recent period of deformation, which

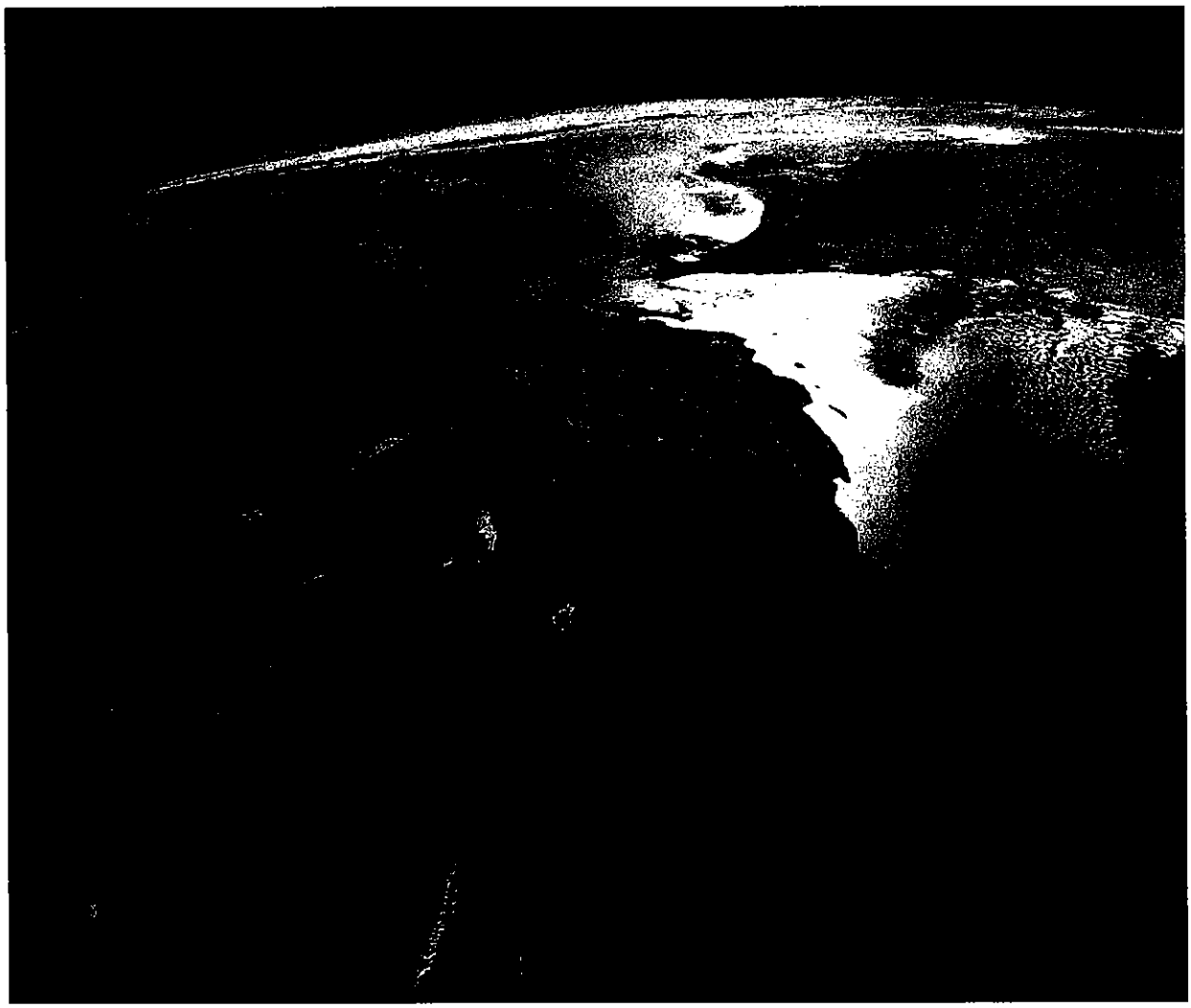

Fig. 4. Space shuttle photograph looking south-east across the southern Zagros Mountains and the Persian Gulf, toward the Straight of Hormuz. Photograph courtesy of NASA.

apparently extends throughout much of Iran, is not well constrained. Berberian & King (1981) estimated that deformation began about 5 Ma, which coincides with the start of a second phase of extension along the Red Sea and Gulf of Aden. If the width of the fold belt (100–200 km) is divided by the duration of folding (5 Myr), the average rate of mountain front advance is between 20 and 40 mm yr^{-1}.*

Compression within the fold belt is manifested by a series of large, doubly plunging folds that verge to the south-west (Fig. 4). Fold wavelengths are on the order of 10 km with amplitudes of up to 2–3 km (Colman-Sadd, 1978; Mann & Vita-Finzi, 1988). As the folds are eroded, their physiography is controlled by variations in the resistance of different sedimentary strata. The regional stratigraphy in the fold belt can be divided into four physiographically effective units (excluding post-Miocene synorogenic sediments) (Fig. 5). From youngest to oldest, these are: (1) erodible evaporites, shales and marls of the Miocene Gachsaran Formation; (2) the highly resistant Oligocene Asmari Limestone, which forms hogbacks around cored folds; (3) a series of erodible late Cretaceous through Eocene flysch deposits, which form valleys where exposed; and (4) a thick sequence of resistant Mesozoic carbonates. As folds are exhumed, variations in the resistance of these strata produce topography characterized by large anticlinal domes (where unbreached Asmari-shelled anticlines protrude from Miocene evaporites), by elliptical Asmari hogbacks encircling breached anticlines and, where exhumation has been greatest, by rugged topography sculpted from Mesozoic carbonates in the inner cores of the anticlines (Oberlander, 1965) (Fig. 4).

Sediment is eroded from the Zagros orogen by a series of transverse streams that either join the longitudinal Tigris–Euphrates river system or flow directly into the

*Mann & Vita-Finzi (1988) used the same approach to estimate a mountain front advance rate, but assumed that deformation began 12 million years ago and so arrived at a value of 17 mm yr^{-1}. For the purposes of this study, the exact value does not matter because the various tectonic parameters are all scaled to the duration of folding.

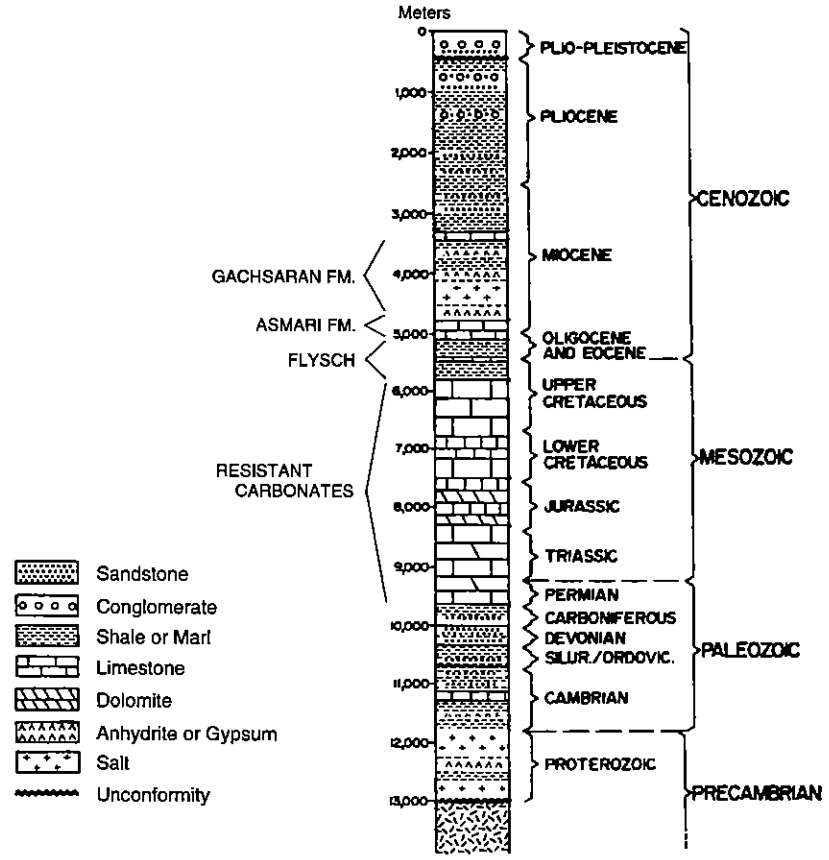

Fig. 5. Generalized stratigraphic column for the Zagros Simply Folded Belt, with the Cretaceous through Miocene interval grouped into four units according to their relative resistance to erosion. Modified from Colman-Sadd (1978).

Persian Gulf (Fig. 3). Unfortunately, a detailed record of late Tertiary to Quaternary sediment delivered to the foreland basin does not presently exist. Plio-Pleistocene synorogenic gravels do, however, show a pronounced late (?) Pleistocene unconformity of regional extent (James & Wynd, 1965; Oberlander, 1965).

In the model, a 42-cell by 82-cell grid with 1-km^2 cells is used to represent an idealized subset of the Simply Folded Belt (Fig. 6, inset). The south-western edge of the grid is maintained at a constant zero elevation. The south-east and north-west boundaries are periodic (that is, they are connected to one another). The north-east boundary is closed to any flow of water and sediment, and represents the edge of the Thrust Zone. Although a number of the transverse streams crossing the Simply Folded Belt actually have their headwaters within the Thrust Zone, for the sake of computational simplicity the presence of such through-going drainage is not accounted for in this study. Results from other model experiments not reported in this study (Tucker, 1996) indicate that the closed-boundary assumption does not significantly alter the outcome of the models, nor does it change the conclusions that are drawn from them. The initial topography for the experiments consists of a planar surface sloping gently (1 m km^{-1}) to the south-west. Small random perturbations ($\pm$0–2 m) are superimposed on this initial surface. The initial stratigraphy consists of four units with differing erodibility (Fig. 6), where erodibility refers to resistance to bedrock channel erosion and is represented by the parameter k_v in Eq. (13). The

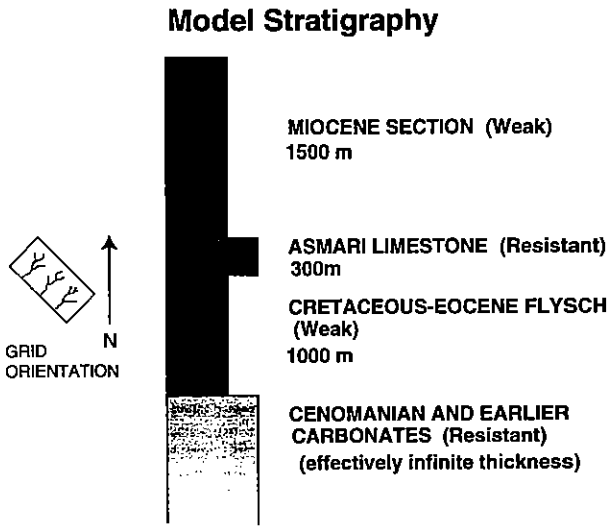

Fig. 6. Stratigraphic column used as an initial condition in the Zagros fold belt simulation. Inset: the orientation of the model grid.

stratigraphic units are: (1) a 1500-m-thick erodible unit corresponding to the evaporites and marls of the Miocene Gachsaran Formation; (2) a 300-m-thick resistant unit, corresponding to the Oligocene Asmari Limestone; (3) a 1000-m-thick weak unit corresponding to Campanian through Eocene flysch (Pabdeh and Gurpi Formations); and (4) a resistant unit of effectively infinite thickness, corresponding to Cretaceous carbonates of the Bangestan group (James & Wynd, 1965). The erodibility of units

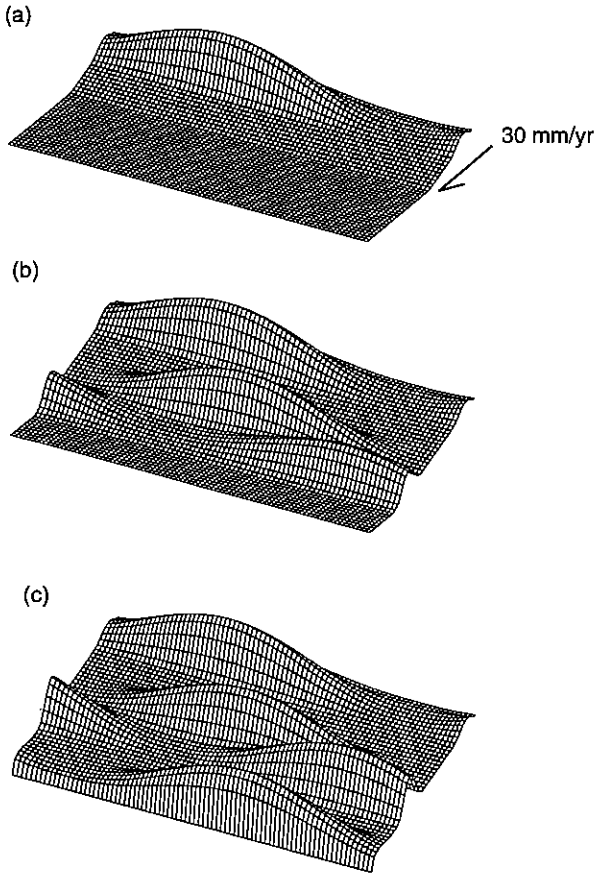

Fig. 7. Uplift function used in the Zagros model experiments. See text for explanation.

(1) and (3), and units (2) and (4), respectively, is assumed to be the same.

To simulate Zagros-style fold tectonics, the initial topography is deformed using the uplift function shown in Fig. 7. Two types of uplift are represented: broad-wavelength regional uplift and, superimposed on this, sinusoidal folding. The presence of broad regional uplift in the Simply Folded Belt is inferred from geological cross-sections, which indicate that the Fold Zone has experienced more rock uplift than can be accounted for by folding of the Palaeozoic sedimentary section alone (Falcon, 1950; British Petroleum Co., 1956, as reproduced in Oberlander, 1965). If the Asmari Limestone is taken as a datum, these cross-sections indicate several thousand metres of uplift relative to the adjacent foreland basin, over and above the uplift on individual anticlines. Gravity modelling (Bird, 1978) and geological evidence (Haynes & McQuillan, 1974) suggest that this additional uplift reflects crustal thickening in a wedge-shaped collision zone accommodated by convergence along blind basement thrusts (Berberian, 1995), as well as a component of isostatic uplift. Because isostatic uplift and subsidence are presumed to be incorporated into the uplift function described below, dynamic flexural isostasy is not computed in this model.

To simulate regional uplift resulting from crustal thickening, and the south-westward propagation of deformation, that portion of the model grid that lies north-east of a 'mountain front' is subjected to uniform uplift at a rate U_b, here set equal to 1 mm yr^{-1} (Falcon, 1969). The mountain front migrates south-westward at a rate of 30 mm yr^{-1} (the average of estimates discussed above) until it reaches the south-western model boundary, at which point the entire grid is subject to uniform uplift. This produces the wedge-shaped background uplift geometry illustrated in Fig. 7. Superimposed on regional uplift are four sinusoidal folds growing in sequence from north-east to south-west (Fig. 7). Fold amplitude, wavelength and peak uplift rate are based on estimates for the Zagros folds (Oberlander, 1965; Colman-Sadd, 1978; Mann & Vita-Finzi, 1988). The positions and timing of the four folds were chosen from a series of simulations in which these parameters were selected at random, with the constraint that the south-westward propagation rate of folding approximately equals the estimated mountain front advance rate of 30 mm yr^{-1}.

Given the uncertainty in the timing of events in the Zagros foreland, the tectonic reconstruction that is described by these boundary conditions is but one of a number of possible scenarios. The purpose of adopting these boundary conditions is not to test a particular tectonic scenario, but rather to provide a set of geologically reasonable conditions as a starting point for modelling. Although the details of the behaviour of the simulations that follow do vary depending upon the choice of tectonic parameters (such as the fold amplitude), the conclusions drawn from the model results do not depend on any one particular tectonic scenario or on any particular set of initial conditions.

MODEL CALIBRATION

The model has three geomorphic parameters which must be calibrated: the erodibility of resistant rocks, k_{vr}, and of weak rocks, k_{vw} (both used in Eq. 13), and the efficiency of sediment transport, k_f (used in Eq. 18). For the case of an active fold and thrust belt, the most reasonable model solutions are those in which the fluvial system is dominated over the long term by bedrock channels, with alluvial channels restricted to structural depressions. In this case, topographic relief is primarily controlled by the dimensionless ratio of tectonic uplift rate to bedrock channel incision efficiency U/k_v, with the sediment transport capacity parameter k_f being a second-order modification. Thus only the two lithologically dependent parameters k_{vr} and k_{vw} need be considered here.

Few studies have attempted to quantify variations in rock resistance to stream incision. Hack (1973a,b) investigated lithological controls on bedrock river profiles in the humid-temperate southern Appalachian highlands. Lithologically controlled gradient variations for some of these streams are listed in Table 1. Along adjacent stream reaches overlying significantly different lithologies, stream gradients vary by anything from a factor of two or three to a factor of nearly 50. Assuming that the downcutting

Table 1. Gradient ratios for adjacent or nearby stream reaches on rocks of varying resistance to channel erosion for selected streams in the central Appalachians. Slopes were computed from the stream gradient indices measured by Hack (1973b).

River	Resistant lithology	Weaker lithology	S_R*	S_W†	Ratio S_R/S_W	Ratio‡ k_{vr}/k_{vw}	Notes
French Broad	granite and massive gneiss	sheared biotite gneiss	4.3	0.45	9.5	4.8	downstream increase
French Broad	granite and massive gneiss	carbonates (Knox Group)	4.3	0.59	7.3	4.0	downstream decrease
Cartecay–Coosawatee–Oostanaula	Low-grade metamorphic rocks (Great Smoky group)	carbonates and clastic sedimentary rocks	11.0	0.23	47.8	15.0	downstream decrease
New River	Resistant sandstone (Pottsville fm)	shale and siltstone (Mauch Chunk fm)	2.2	0.74	2.9	2.1	downstream increase

* S_R = channel gradient on resistant lithology (m km^{-1}). † S_W = channel gradient on weaker lithology (m km^{-1}). ‡ Computed from Eq. (19), assuming $n = 2/3$.

rates are equal for adjacent reaches and that discharge varies little between these reaches, the gradient ratios can be related to the rock erodibility ratio by

$$\frac{k_{vw}}{k_{vr}} = \left(\frac{S_R}{S_W}\right)^n \tag{19}$$

where S_R and S_W are the gradients on resistant and weaker lithologies, respectively, and n is the exponent in Eq. (13). Although the gradient ratios on these humid-temperature streams are not directly applicable to arid settings in which carbonates act as the resistant caprocks, they do provide a general guide to the degree of natural variation in erodibility in a landscape where lithology is important in shaping topography. It is likely that in arid regions such as the Zagros, where lithology clearly exerts a first-order control on landforms, rock erodibility variations are at least as large as those observed in humid-temperate environments such as the Appalachians.

In the absence of better constraints on rock erodibility, a 10-fold contrast between erodible and resistant lithologies is herein assumed (that is, $k_{vr}/k_{vw} = 10$). Models using lower values of k_{vr}/k_{vw} fail to reproduce the characteristic erosional topography of the Zagros Simply Folded Belt, whereas models that assume a 10-fold or higher contrast do a good job of reproducing the elliptical hogbacks and centripetal or axial fold valleys that are so common in the Zagros landscape (Oberlander, 1965) (Fig. 4).

The absolute values of the parameters k_{vr} and k_{vw} are calibrated by comparing predicted and observed topographic relief (Fig. 8). Several runs were computed in which only k_{vr} and k_{vw} were varied. The topographic relief after 5 Myr of simulation time was then compared to the observed relief (Fig. 8). Given the lithological and tectonic boundary conditions described above (Table 2), and assuming $k_{vr}/k_{vw} = 10$, values of k_v less than about 0.07 m yr^{-1} (for erodible rocks) and 0.007 m yr^{-1} (for resistant ones) produce excessively high relief, while values much greater than 0.4 and 0.04 m yr^{-1}, respectively, produce significantly lower relief than is observed. Consequently, values of $k_{vr} = 0.02$ m yr^{-1} and $k_{vw} = 0.2$ m yr^{-1} are used in the experiments described below.

RESULTS AND DISCUSSION

Morphotectonic evolution

The first simulation of the Zagros fold and thrust belt represents a scenario in which folds grow serially from north-east to south-west at a rate of 30 mm yr^{-1} (the average mountain front advance rate discussed above), with a maximum fold crest uplift rate of 1 cm yr^{-1}. Once fold growth has ceased, the landscape remains subject to uniform uplift at a rate of 1 mm yr^{-1} due to crustal thickening at depth, while the south-western boundary elevation remains fixed.

As uplift and folding commence, a series of parallel streams form in the lowlands ahead of and between the rising folds (Fig. 9a). (Note that for clarity only the larger streams are sketched in Fig. 9; in the model, every grid cell contains a channel.) Debris transported from the rising highlands by low-order streams (not shown) accumulates in an alluvial apron immediately basinward of the mountain front, with deposition also occurring in the syncline between the two folds (Fig. 9a). Mesozoic carbonates are exposed in the core of the oldest fold, while erosion has not yet stripped the younger fold of its Miocene cover (Fig. 9a). As the mountain front migrates, new folds arise and the drainage pattern adjusts accordingly (Fig. 9b). (Drainage adjustment and the mechanics of water gap formation in these simulations will be the subject of a separate, forthcoming report.) Sediment previously deposited is remobilized and transported further into the basin; at this point, significant synorogenic deposits occur in only a few structural lows. Because of the large fold amplitude in this experiment, the resistant Asmari Limestone carapace is quickly penetrated along the anticlinal crests, exposing the underlying strata to erosion (Fig. 9b). This produces topography characterized by resistant hogbacks rimming the inner anticlinal cores (albeit discontinuously in this example as a result of the model's coarse resolution).

As uplift continues, the drainage networks adjust to the structure and lithologies by forming a trellis drainage pattern (Fig. 9c). Streams begin to exploit the erodible

© 1996 Blackwell Science Ltd,

Table 2. Model parameter values for Experiment 1.

Description	Parameter	Value
MODEL DOMAIN		
Grid size	—	42 by 82 cells
Cell width	Δx	1 km
SURFACE PROCESSES		
Bedrock channel erosion rate	E_b	$k_v(Q/Q^*)^{0.3}S^{0.7}$
Erodibility of a weak lithology	k_{vw}	0.23 m yr^{-1}
Erodibility of a resistant lithology	k_{vr}	0.023 m yr^{-1}
Sediment transport efficiency	k_f	0.1
Effective precipitation rate	P	1 m yr^{-1}
TECTONIC PARAMETERS		
Background uplift rate	U_b	1 mm yr^{-1}
Mountain front advance rate	V_u	0.03 m yr^{-1}
Number of folds	—	4
Fold wavelength	λ	10 km
Fold length along strike	λ_s	75 km
Maximum fold Amplitude	α_f	2500 m
Fold crest uplift rate	U_f	0.01 m yr^{-1}
Fold locations*		
Fold #1	—	(37,53)
Fold #2	—	(22,40)
Fold #3	—	(15,13)
Fold #4	—	(3,30)
Onset of folding†		
Fold #1	t_{f1}	160 kyr
Fold #2	t_{f2}	590 kyr
Fold #3	t_{f3}	870 kyr
Fold #4	t_{f4}	1100 kyr
INITIAL CONDITIONS		
Initial surface slope	—	1 m km^{-1}
Amplitude of random elevation variations	Δh_r	$\pm$2 m
Thickness of uppermost lithology (weak)	T_1	1500 m
Thickness of 'Asmari Limestone' (resistant)	T_2	300 m
Thickness of 'flysch' horizon (weak)	T_3	1000 m
Thickness of 'Mesozoic' section (resistant)	T_4	∞

*Given in kilometres from the left edge and bottom edge of the grid, respectively. †Time at which fold uplift begins, in model years from the start of the simulation.

flysch where it is exposed between the outer Asmari hogbacks and the inner fold cores. By this point, previously deposited synorogenic sediments have been completely stripped from the landscape. Stream erosion has also stripped off the Miocene marls and evaporites within most of the valleys, exposing the underlying resistant Asmari Limestone (Fig. 9c).

With further uplift and exhumation, the drainage network continues to adjust to the changing outcrop pattern (Fig. 9d). Sediment accumulations are negligible, except for a few discontinuous patches. The Asmari Limestone unit has been stripped off of the landscape, with isolated remnants forming synclinal hills (Fig. 9d).

Sediment flux evolution

Figure 10 gives the sediment flux curve produced by this morphotectonic evolution. Sediment flux grows monotonically with time, following the tectonic uplift curve but lagged by about 400 000 years. At 1.2 Myr, the sediment flux has reached a maximum, now lagging only ~200 000 years behind the time of maximum average uplift rate. Sediment flux from the fold and thrust belt now declines, not only because fold growth has stopped, but also because of increasingly widespread exposure of resistant rocks. The small reversal on the falling limb of the first peak results from a temporary acceleration in erosion as the erodible flysch unit is exposed in the core of the outermost fold. Stripping of the resistant Asmari Limestone is associated with a second peak in sediment supply (Fig. 10). Finally, with the removal of most of the flysch, the sediment supply is once again diminished. It begins to rise again as continuing uplift increases the topographic relief, which produces an increase in denudation rate. The sediment outflux would eventually come into equilibrium with the tectonic mass influx rate if the simulation were continued.

The sediment flux variations shown in Fig. 10 arise primarily from variations in tectonic uplift rate and in rock resistance. The first peak in sediment supply results from the initial pulse of uplift associated with outward expansion of the mountain front and rapid fold growth. The curve resembles typical sediment yield curves seen in experimental data and in natural settings at a variety of scales (Schumm & Rea, 1995), and shows only a small lag and attenuation of the sedimentary response to this initial uplift. In the example of Fig. 10, the presence of a thick (1500-m) succession of erodible strata at the onset of uplift allows for a rapid sedimentary response to the imposed tectonic uplift. Such an initially rapid response may in fact be a common feature of the early collisional phase of orogens, where erodible trench sediments are thrust upward to form a subaerial mountain range. Exactly how rapid such a response might be depends on the geomorphic response time, which in turn is a function of rock erodibility, climate and (possibly) uplift rate. The geomorphic response time is crucial because it determines the degree to which sediment pulses resulting from episodic uplift will be attenuated – the longer the response time, the greater the attenuation (cf. Kooi & Beaumont, 1996). If the response time were much longer than the time scale of tectonic forcing, the uplift signal would be strongly attenuated and episodic thrusting (for example) would not show up in the stratigraphic record. On the other hand, if the geomorphic time scale were less than or commensurate with the time scale of tectonic forcing, then episodic uplift would be much more likely to be recorded in a basin. Episodic uplift would be most strongly recorded in proximal terrestrial or nearshore deposits (Shanley & McCabe, 1994).

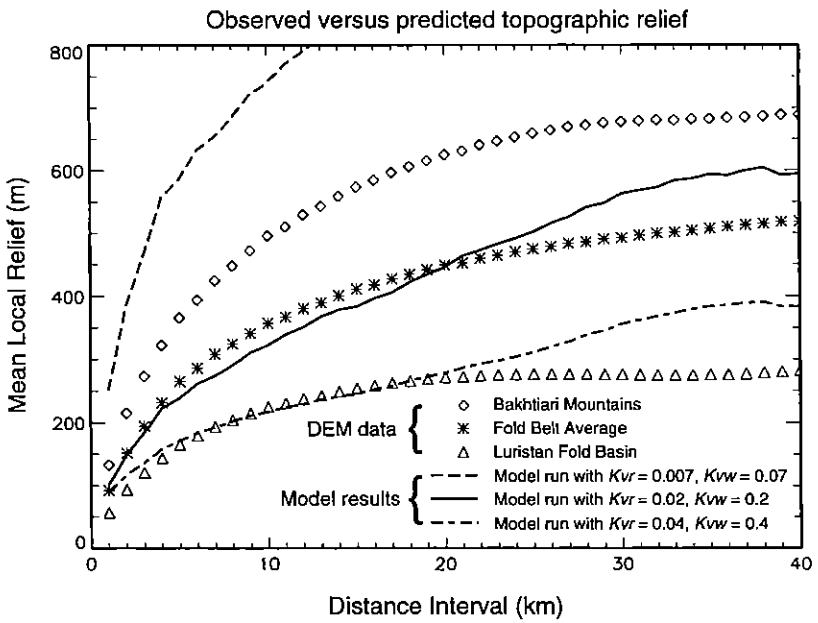

Fig. 8. Relief for three different model experiments (lines) compared with observed relief in the Central Zagros Mountains (symbols). Relief was computed from a 1 km digital elevation model (DEM) of the Central Zagros region, and represents the mean elevation difference between points spaced a given distance interval apart. The highest relief in the Central Zagros occurs in the Bakhtiari Mountains (diamonds), and the lowest relief occurs in the Luristan Fold Basin to the northwest (triangles) (Fig. 2). (A discussion of the various structural provinces in the Central Zagros is given by Oberlander, 1965.) Curves for the models represent the topographic relief after 5 Myr of simulation time, which is equivalent to 5 km of background tectonic uplift. Values listed for k_v represent values for the resistant (k_{vr}) and erodible (k_{vw}) lithologies, respectively. Of the three simulations pictured, only the middle one falls comfortably within the range of observed topographic relief.

Results from simple one-dimensional model experiments suggest that for a landscape dominated by bedrock-floored channels, assuming that the effective precipitation rate is constant, the time required to reach equilibrium with a given rate of uplift will be proportional to the rock erodibility, k_v, the width of the uplifted region, L, and the uplift rate, U, according to

$$T_s \propto \frac{U^{((1/n)-1)}L}{k_v^{(1/n)}} \tag{20}$$

where n is the exponent on the slope term in Eq. (13). The response time for models calibrated against the Zagros relief data can be interpreted in light of this relationship. Using the calibrated values of k_v (Fig. 8), geomorphic response times (defined as the time required to reach 90% of the equilibrium sediment flux) are on the order of 0.1–0.15 Myr for the erodible lithologies, and 3–4 Myr for the resistant ones, assuming a constant uplift rate of 1 mm yr^{-1}. By comparison, the interval between episodes of activity on thrusts documented in the western Himalaya by Burbank & Raynolds (1988) is on the order of 1–3 Myr. (Unfortunately, to the best of the authors' knowledge a similar study has not been done for the Zagros folds and thrusts.) Thus, the calibrated values for a 40-km-wide model suggest geomorphic response times for resistant lithologies that are roughly commensurate with, or slightly longer than, the timing of thrusting in at least one orogenic belt. Because the response time also scales with the width of the uplifted region, narrower thrusts should show a faster response and thus be more susceptible to producing discrete pulses of sediment in an associated basin.

The delay between the onset of uplift and the ensuing sediment pulse in the model results in part from temporary sediment storage in an alluvial apron immediately basinward of the expanding mountain front (Fig. 9). Sediment accumulates in this mountain front alluvial plain until the stream slopes become large enough to transport material derived from the rising highlands all the way out to the fixed base level, which in this case could represent either a shoreline or a major structural boundary, such as the Zagros Mountain Front blind thrust fault described by Berberian (1995). This feature of the model results suggests a mechanism for the apparent delay between uplift of the Tibetan Plateau, some time before 14 Ma (Coleman & Hodges, 1995), and the onset of rapid sedimentation in the northern Indian Ocean at ~ 12 Ma (Rea, 1992). If the India–Asia collision did indeed produce significant uplift well before ~12 Ma, the delay between this event and the sedimentary signal in the Indian Ocean probably reflects a time during which sediment was trapped in the proto-Ganges/Brahmaputra foreland basin, filling the basin until alluvial gradients became sufficient to allow sediment to bypass the basin and spill over into the northern Indian Ocean.

Lithological controls on sediment supply

As the first erodible horizon is stripped from the model landscape, the sediment flux drops below the rate of tectonic mass influx (Figs 9c and 10). The decrease is followed by a gradual increase as stream profiles adjust to the newly exposed resistant rocks. Like natural streams, the model streams seek an equilibrium profile, which in

© 1996 Blackwell Science Ltd,

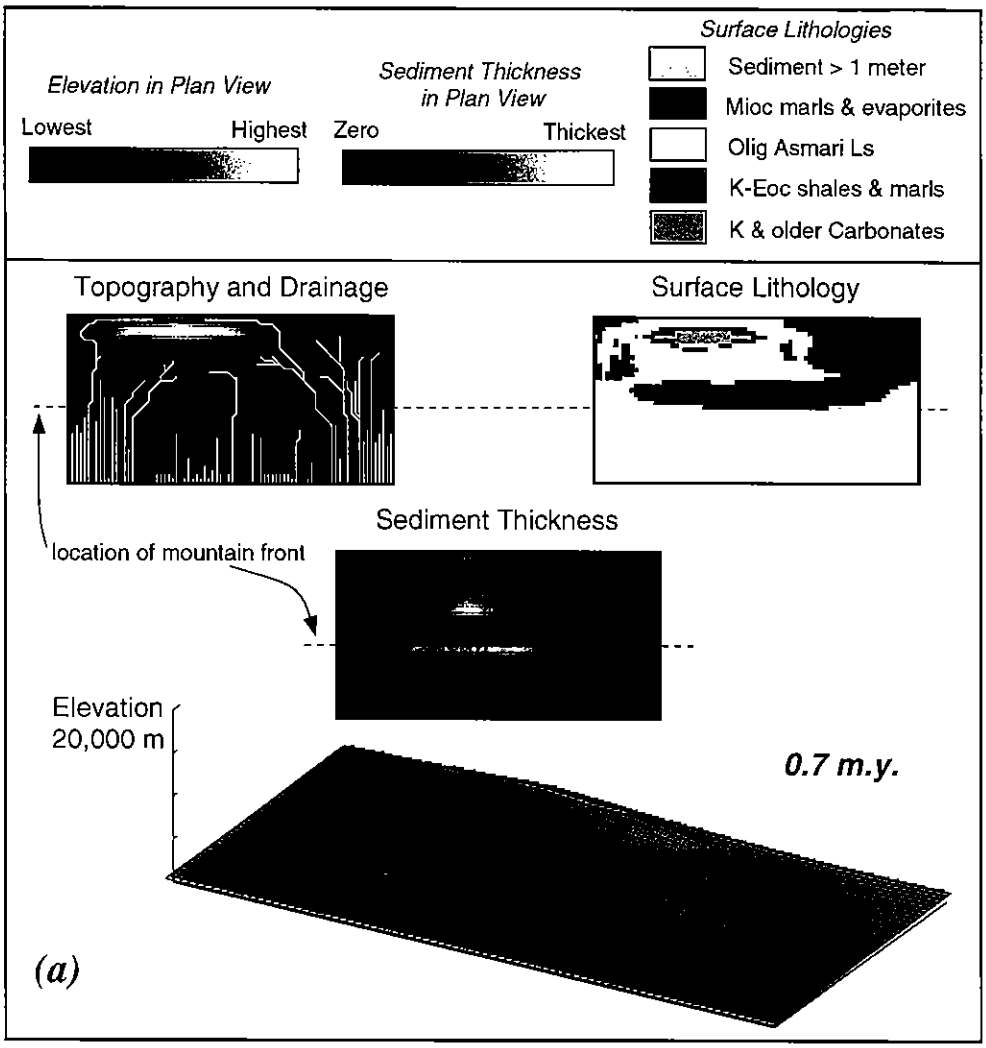

Fig. 9. Results of the first model run, showing the evolution of topography, drainage patterns and surface lithologies. On the drainage pattern maps, only stream segments having an upstream drainage area greater than 20 model cells (= 20 km^2) are shown. (a) Simulation at 0.7 Myr, showing sediment accumulation in an alluvial apron ahead of and between the growing folds. (b) Simulation at 1.2 Myr, corresponding to the time of peak sediment flux (see Fig. 10). (c) Simulation at 2.6 Myr, corresponding to the first lithologically produced lag in sediment supply. Most of the landscape at this point is underlain by resistant lithologies. (d) Simulation at 3.4 Myr, corresponding to the second peak in sediment supply. The surface geology is dominated by the erodible flysch unit. Note the presence of residual topography formed on remnants of the resistant Asmari Limestone unit within the synclines.

this case is that profile which provides just sufficient energy to lower the channel bed at a rate equal in magnitude to the local tectonic uplift rate. For the case of bedrock streams, Eq. (13) implies that at equilibrium the uplift and downcutting rates are equal:

$$U = k_v \left(\frac{Q}{Q_*}\right)^m S^n. \tag{21}$$

This in turn implies that equilibrium channel gradients are a function of the uplift rate, the rock erodibility and the effective discharge, according to

$$S = \left(\frac{U}{k_v}\right)^{1/n} \left(\frac{Q}{Q_*}\right)^{-m/n}. \tag{22}$$

A similar relationship exists for capacity-limited alluvial channels (see Willgoose *et al.*, 1991, for a discussion of the equilibrium slope-discharge relationship in this type of model).

All else being equal, a change in rock resistance (k_v) during exhumation will produce a corresponding change in the equilibrium profile, and bedrock streams that are subject to uplift will respond to such a change by adjusting their incision rates until the new equilibrium profile is established. The first decline in sediment flux in the model example (Fig. 10) results from a decrease in rock erodibility as the first resistant stratum is progressively exposed. Sediment yield begins to rise again as river profiles steepen to approach a new equilibrium with the resistant lithology and as the proportion of resistant rocks exposed at the surface declines (Fig. 10). This is followed by an overshoot in sediment flux (Fig. 10) as the now-steepened stream profiles penetrate the resistant unit to expose the underlying erodible unit (correspond-

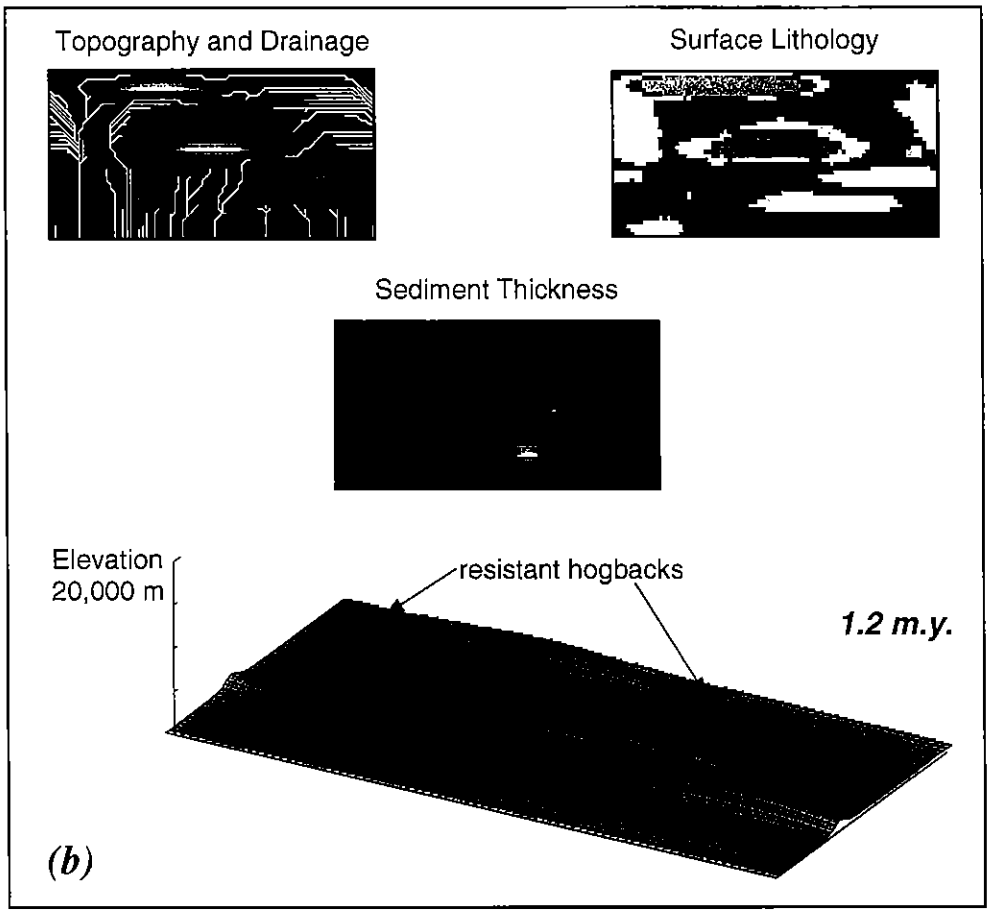

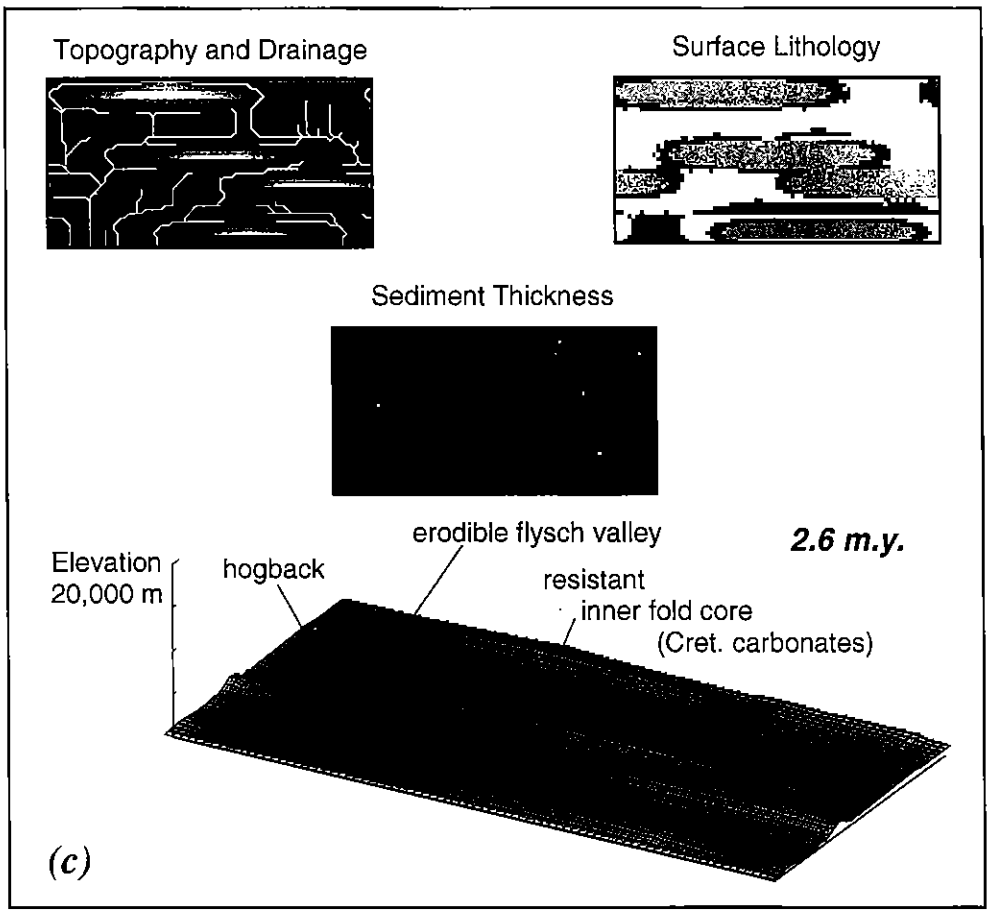

Fig. 9. (*continued*)

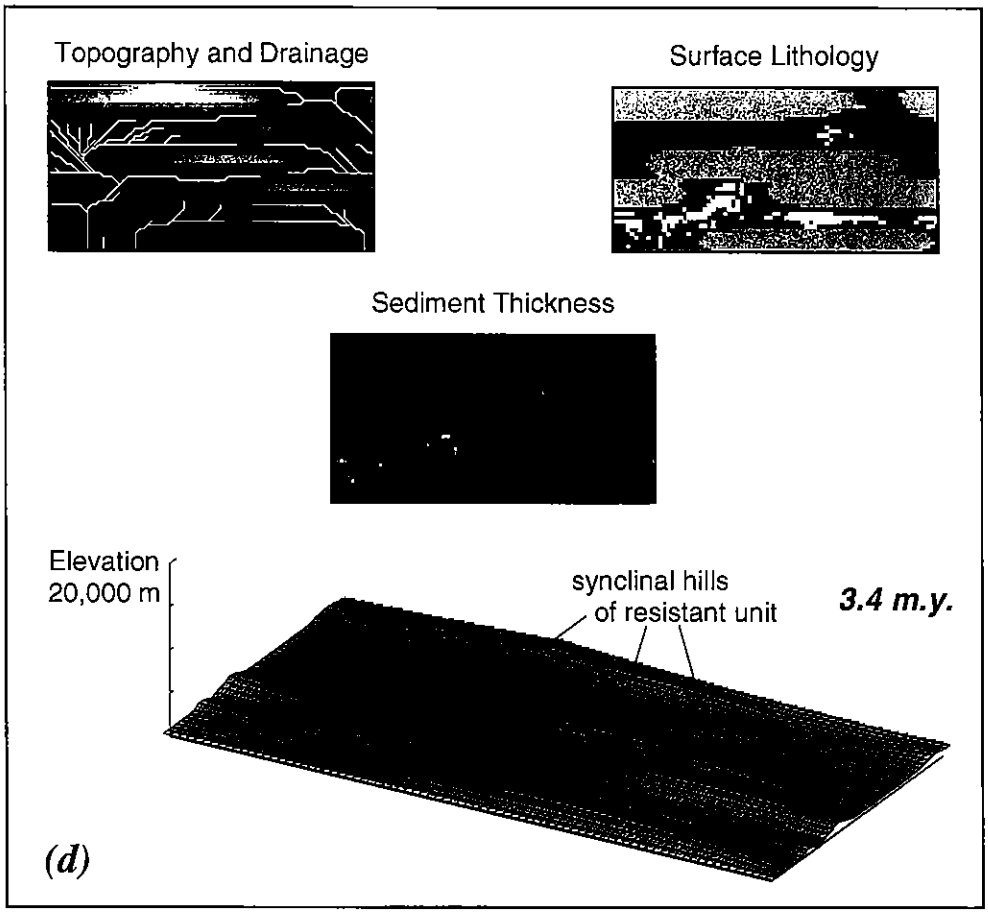

Fig. 9. (*continued*)

ing to Cretaceous–Eocene flysch). A similar sequence of events follows as the next resistant group of resistant rocks (Mesozoic carbonates) is exhumed (Fig. 10). The timing of these lithological variations scales with the ratio of stratal thickness to rock uplift rate.

The magnitude of lithologically generated sediment-supply variations will be a function of the degree of variation in rock resistance, the degree of internal deformation in the source terrain and the thickness of similarly resistant rock units. A quantitative description of rock resistance variations is presently lacking; however, the obvious importance of lithology in shaping the topography of many orogens, including the Zagros, suggests that such variations can be considerable. This contention is supported by a recent study of erosion and sedimentation along the western Gulf of Suez (Steckler & Omar, 1994), where the exposure of easily eroded friable sands beneath a competent limestone unit appears to have initiated rapid scarp retreat and a concomitant increase in the rate of sediment delivery to the Gulf of Suez rift basin.

The importance of rock resistance variations depends also on the degree of internal deformation in the source terrain. Intense folding and faulting will tend to juxtapose many different lithologies at the surface, thereby diminishing the potential for significant lithologically controlled sediment-flux variations. The greatest potential for lithological control of denudation and sedimentation occurs where flat lying or gently dipping strata are subject to coherent block uplift, as in the case of Rocky Mountain-style block uplifts or rift shoulder uplifts. This is illustrated by a model run in which the same stratigraphic section used in the previous model (Fig. 6) is subject to uniform block uplift without folding. In this case, sediment supply fluctuates considerably (Fig. 11) as strata of different resistance are progressively exhumed, even though the rock uplift rate remains constant.

Stream capture and shifting depocentres

Drainage patterns in orogens often shift in response to folding, thrusting and rock-type variations as the orogen is exhumed (e.g. Oberlander, 1965, 1985; Burbank & Raynolds, 1988; Jolley *et al.*, 1990; Burbank & Verges, 1994). Major changes in drainage patterns resulting from stream diversion and/or capture can produce corresponding changes in the location and magnitude of sediment point sources. Such a mechanism has been invoked to explain rapid facies shifts and changes in shoreline position (e.g. Martinsen *et al.*, 1993; Schlager, 1993). The effect of stream capture on the location and magnitude of sediment point sources is illustrated by a numerical experiment shown in Fig. 12. Here, drainage has initially been diverted around either side of a large fold, producing three primary drainage basins (Fig. 12a) and

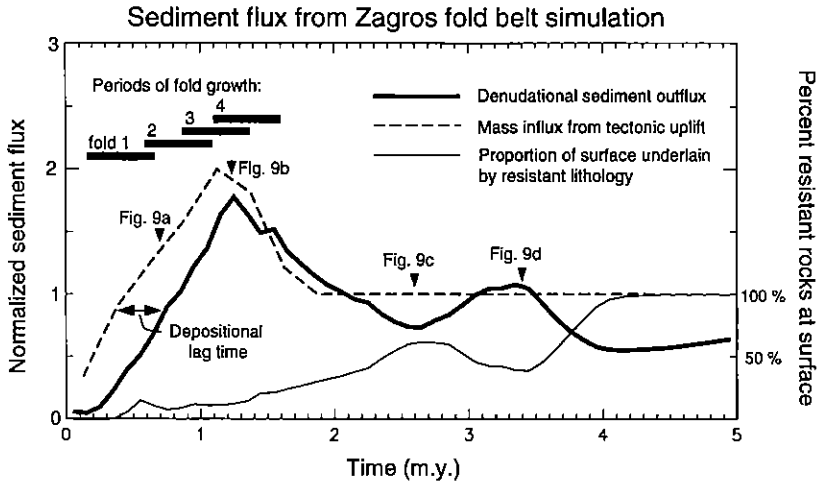

Fig. 10. Total sediment flux out of the grid versus time for the model experiment shown in Fig. 9. Thick solid lines show the periods of growth for each of the four folds. Note the time lag between the onset of uplift and the initial sedimentary response. The decline and subsequent increase in sediment supply at 2–3 Myr reflect changes in the proportion of resistant versus erodible rocks exposed at the surface.

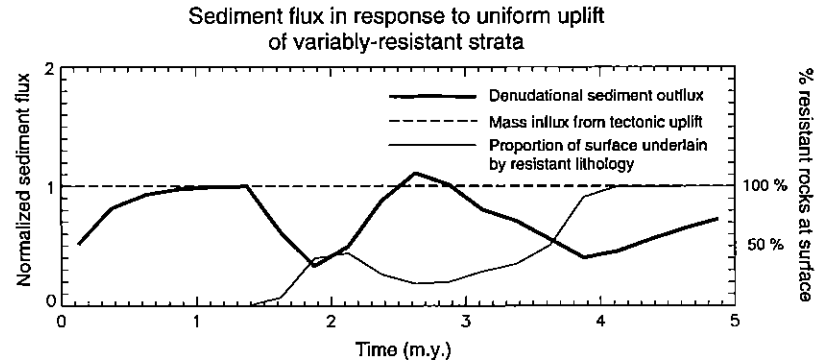

Fig. 11. Sediment flux through time for an experiment in which the stratigraphic column used in the previous experiment (Fig. 6) is subjected to spatially and temporally uniform uplift. Sediment supply variations are solely the result of lithological variations.

two corresponding primary depocentres (Fig. 12b). A water gap has been carved where a third fold has begun to grow beneath the right-hand stream (Fig. 12a). As this fold continues to grow, the right-hand stream is deflected by the fold and captured by the adjacent drainage basin (the left-hand basin in Fig. 12c; recall that the left and right model boundaries are joined, so that the right-hand stream in Fig. 12c crosses over to the opposite boundary). This capture event is accompanied by the disappearance of the first basin as a sediment source point, and a large increase in the sediment delivery rate at the outlet of the left-hand drainage basin (Fig. 12c,d).

Occurrences of stream diversion by folds or emergent thrusts are common in orogens (e.g. Jolley *et al.*, 1990; Burbank & Verges, 1994; Talling *et al.*, 1995). The significance of such diversion for basin stratigraphy depends upon the scale of the drainage pattern shift, which in turn depends upon the scale of the structures involved. With large structures, such as the Kabir Kuh anticline in the Zagros or the Salt Range thrust in the Western Himalayas, there exist the potential to shift large drainages by tens to hundreds of kilometres.

Sediment ponding

In intermontane basins, where external drainage has been deflected or cut off altogether, temporary ponding and later evacuation of sediment has the potential to create significant variations in sediment supply. The timing of such variations may in fact be independent of any direct tectonic controls, reflecting instead the time required for stream incision to 're-open' drainage in a closed intermontane basin (e.g. Kooi & Beaumont, 1996). In the model examples presented so far, sediment ponding has had a relatively minor effect. The limited extent of sediment ponding in the simulations presented so far reflects the limited lateral extent of the folds – the folds simply are not long enough to trap much debris. By comparison, in the Zagros fold and thrust belt, thick accumulations of synorogenic gravel (the Pliocene upper Agha Jari Formation and Plio-Pleistocene Bakhtiari Formation) are rare within the smaller synclines, but common within structural troughs associated with the larger structures, as well as along the outer mountain front where these deposits reach considerable thickness (James & Wynd, 1965; Oberlander, 1965).

The next experiment addresses a case in which structures are more laterally continuous than those considered so far. The experiment explores the case of sediment ponding in response to episodic uplift on two thrusts separated by a 20-km-wide 'intermontane basin'. Each thrust is represented by a 10-km-wide block subject to spatially uniform uplift. The uplift rate of 1 cm yr^{-1} falls within the typical range of values estimated for folds and thrusts (e.g. Burbank & Raynolds, 1988; Rockwell *et al.*, 1988), and the rock erodibility is set equal to the 'hard rock' value estimated from the Zagros relief data (Table 3). The model is subjected to three 500 000-year-

© 1996 Blackwell Science Ltd,

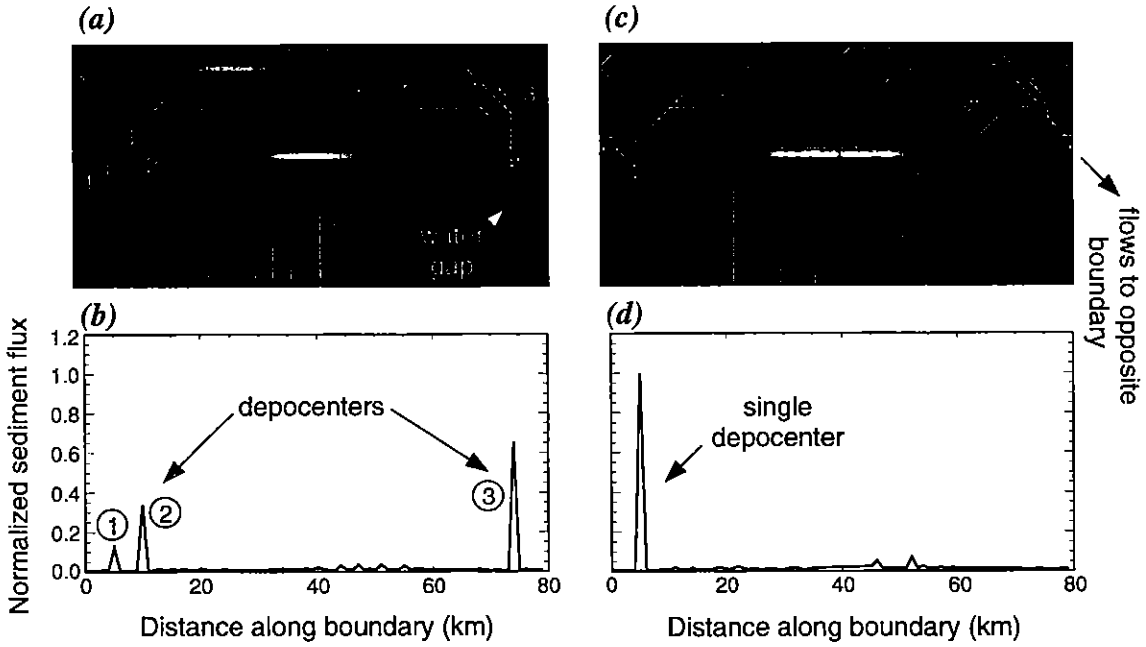

Fig. 12. Example of changes in the location and magnitude of depocentres due to stream capture. (a) Topography and drainage at Time 1. Drainage has been deflected around the centermost fold, producing three primary drainage basins. The right-hand stream has carved a water gap across the growing fold in the lower right. (b) Sediment flux along the lower model boundary at Time 1, showing two primary depocentres associated with the left-hand (1 and 2) and right-hand (3) drainage basins. (c) Topography and drainage pattern at Time 2. The right-hand stream has been deflected by the fold and captured by the left-hand basins across the reflective lateral model boundary. The two left-hand basins have also amalgamated into one. (d) Sediment flux across the lower boundary following stream capture. The right-hand depocentre has been abandoned and the sediment feed rate at the left-hand depocentre has increased by about a factor of two.

Table 3. Model parameter values for thrust experiment.

Description	Parameter	Value
SURFACE PROCESSES		
Rock erodibility	k_v	0.023 m yr^{-1}
Sediment transport efficiency	k_f	0.1
TECTONIC PARAMETERS		
Uplift rate on thrusts	U	0.01 m yr^{-1}
Thrust timing:		
Uplift on inner thrust	—	0–0.5 Myr
No activity	—	0.5–1.5 Myr
Uplift on outer thrust	—	1.5–2 Myr
No activity	—	2–3 Myr
Uplift on inner thrust	—	3–3.5 Myr
No activity	—	3.5–4.5 Myr

long pulses of uplift, each followed by a 1-Myr period of quiescence: (1) initial uplift on the hinterland (inner) thrust; (2) uplift on the basinward (outer) thrust; (3) renewed (out-of-sequence) uplift on the inner thrust.

The results of initial uplift along the hinterland thrust (Fig. 13a) are predictable enough: erosion along the edge of the thrust and establishment of transverse drainage across a sloping alluvial plain. Uplift along the basinward thrust then cuts off the previously established drainage, creating a closed basin that fills with sediment derived from both structures (Fig. 13b). This basin is analogous to the Kashmir Basin between the Pir Panjal and Great Himalayan Ranges (Burbank & Raynolds, 1988). Like the Kashmir Basin, drainage within the closed basin in Fig. 13(b) consists of primary longitudinal streams that are fed by shorter transverse streams draining the two flanking highlands. Because the basinward thrust has cut off the previously established transverse drainage, it actually produces a decrease rather than an increase in sediment flux (Fig. 14). At this point, sediment delivered to the outer edge of the model (the foreland basin) derives solely from one flank of the outer thrust range. Renewed uplift on the hinterland thrust does not produce an increase in sediment supply to the foreland basin (Fig. 14). Instead, this out-of-sequence uplift adds sediment to the intermontane basin and causes the longitudinal drainage axis within the intermontane basin to shift toward the outer thrust. Ultimately, headward erosion along two streams draining the flank of the outer thrust re-opens the intermontane basin at two sites (Fig. 13c), producing a large pulse of sediment (Fig. 14). The timing of this sediment pulse corresponds to none of the three episodes of uplift. Thus, this example illustrates the potential for a significant mismatch between tectonic activity and sediment supply in the distal parts of a foreland basin, especially in cases where deformation in the source terrain is characterized by episodic activity on large thrusts.

Episodic activity on the two thrusts in this example is reflected in the synthetic stratigraphic architecture and

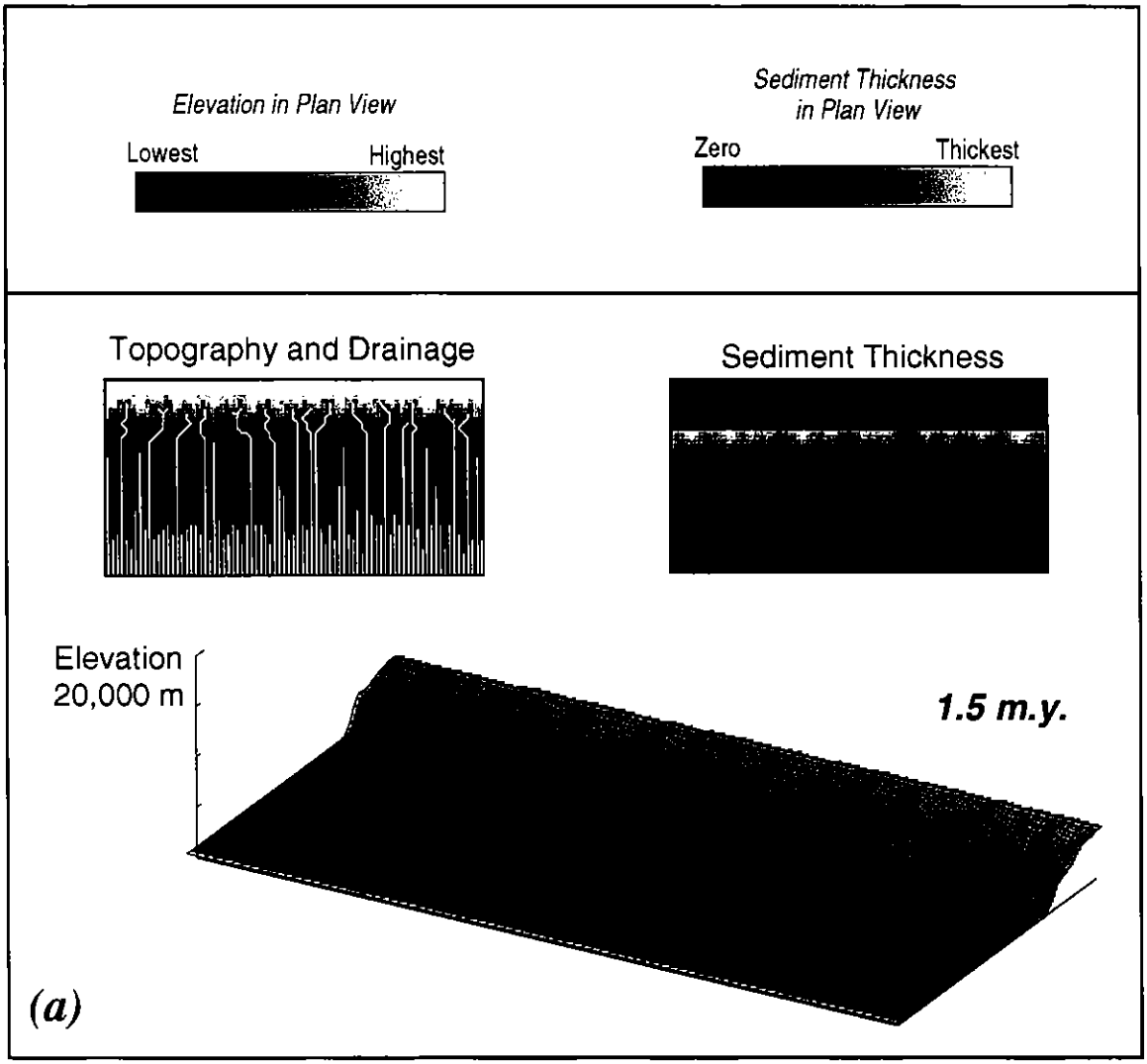

Fig. 13. Topography, drainage and sediment accumulation pattern for a model experiment that explores the effect of block uplift along two 'thrusts'. (a) Simulation at 1.5 Myr, following the cessation of uplift on the first thrust. (b) Simulation at 2.5 Myr, after transverse drainage has been cut off by the second thrust. Sediment ponds in an intermontane basin, backfilling valleys incised into the inner thrust. (c) Simulation at 4 Myr, following renewed uplift on the inner thrust. The intermontane basin has been breached by headward erosion along two streams draining the flank of the outer thrust.

palaeocurrent orientations of the resulting intermontane basin deposits (Fig. 15). The longitudinal drainage axis gradually shifts landward (to the right in Fig. 15) during and following growth of the outer thrust. During the second episode of uplift on the inner thrust, the longitudinal drainage axis shifts rapidly basinward again (to the left in Fig. 15).

Implications for general-purpose basin fill models

Is it really necessary to use a complicated drainage basin model in order to properly model sediment supply rates? Could not sediment supply instead be described using a simpler set of empirical relationships between sediment flux and such variables as relief, uplift, lithology and climate? We suggest that the answer to both questions is yes. The fold and thrust belt simulations presented above imply that the simplest empirical relationships suggested by sediment yield studies may not be adequate for fold and thrust belt settings. Consider, for example, the well-known correlation between sediment yield and topographic relief (e.g. Schumm, 1963; Ahnert, 1970; Milliman & Syvitski, 1992; Summerfield & Hulton, 1994). Topographic relief is certainly an important controlling variable in the numerical model, yet the simulations do not show a simple monotonic relationship between relief and sediment flux (Fig. 16). Instead, there are periods when the two signals are out of phase with one another. In the example shown in Fig. 16, this arises primarily from lithological variation: when softer rocks are exposed, accelerated erosion dissolves away relief while producing an increase in sediment yield, and the reverse occurs when resistant rocks are exposed. We suggest that such lithological controls are responsible for part of the scatter observed in sediment yield studies. A

© 1996 Blackwell Science Ltd,

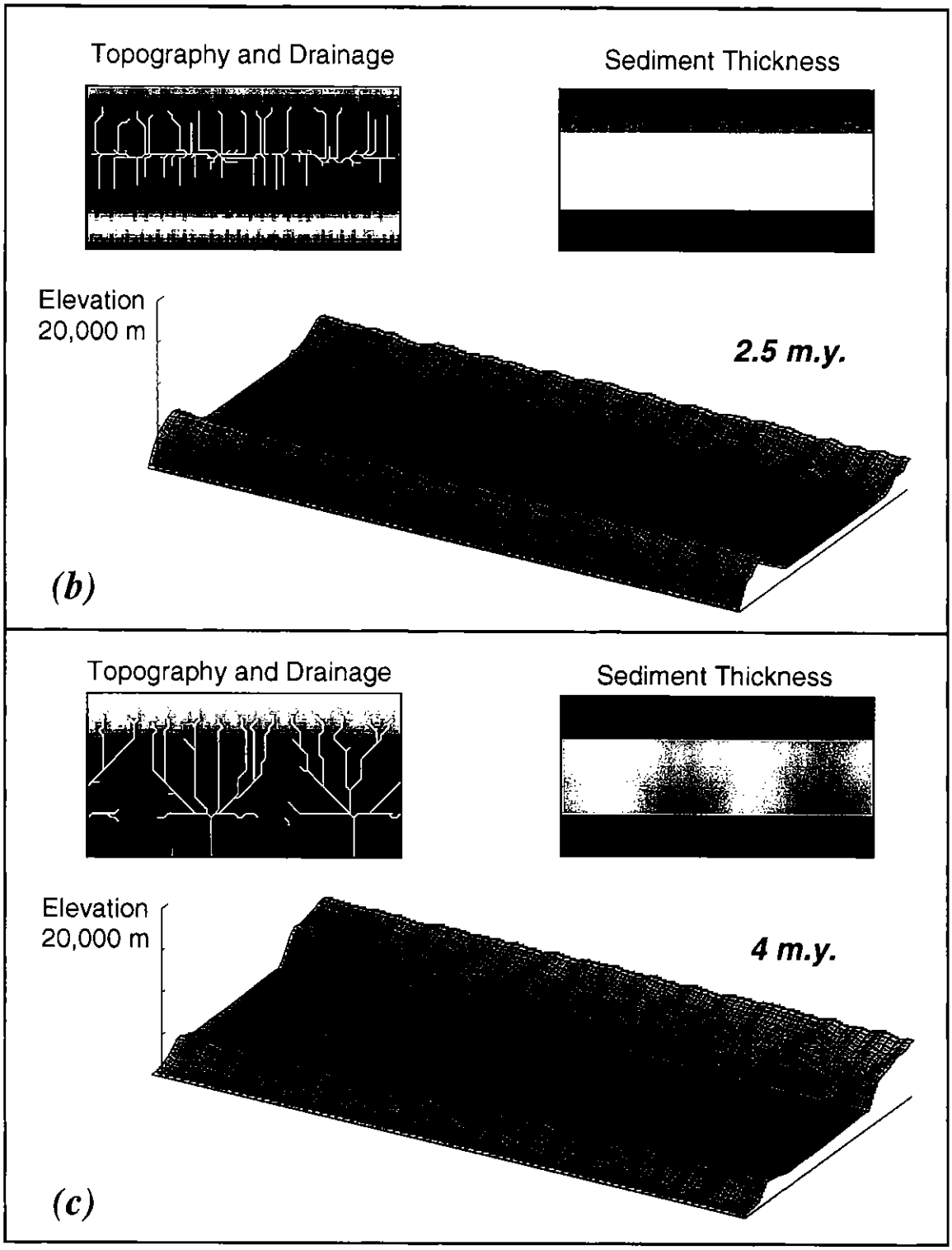

Fig. 13. (*continued*)

simple sediment-flux model based only on topographic relief would fail to capture the lags and phase offsets associated with lithological and other effects, thereby potentially missing an important part of the story. We conclude that while it may not ultimately be necessary to solve the complete, linked uplift–erosion–sedimentation problem in basin-fill models, the problem needs to be addressed in some detail before simpler relationships between sediment flux and its controlling variables can be derived.

CONCLUSIONS

Coupled models of tectonic uplift, fluvial erosion and deposition highlight several potentially significant morphotectonic controls on basin sediment supply. For scen-

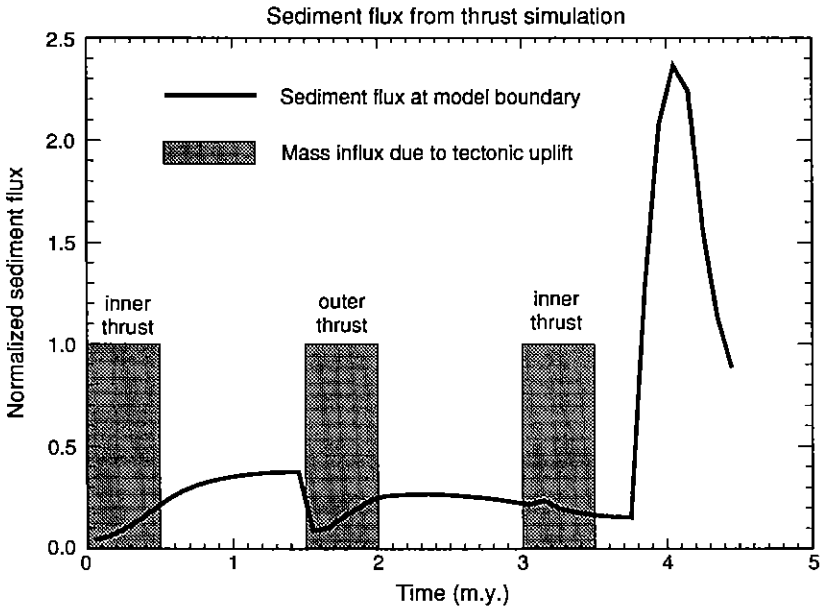

Fig. 14. Sediment flux through time for the thrust experiment shown in Fig. 13. The large peak in sediment flux occurs when headward-eroding streams penetrate the intermontane basin.

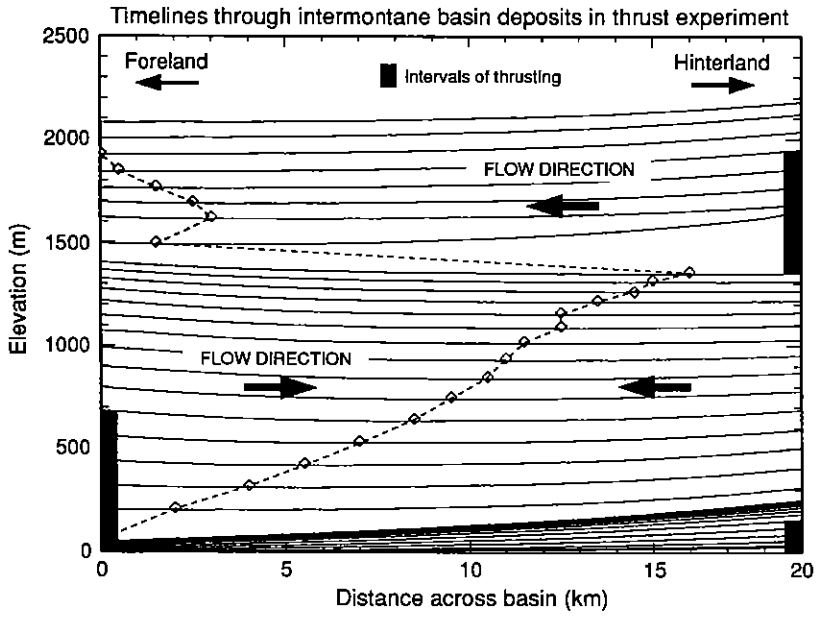

Fig. 15. Synthetic stratigraphic section showing time lines and sediment dispersal directions for the intermontane basin in the thrust simulation (Fig. 13). The section is taken across the centre of the basin, perpendicular to strike, at the time of maximum basin fill. The three episodes of thrusting are reflected in the migration of the position of the longitudinal stream, which is shown by the diamonds.

arios in which deformation migrates progressively basinward, as in the Zagros Mountains, models show a delay between the onset of uplift and the ensuing sediment flux response. This delay reflects the time required for sediment from the rising highlands to accumulate in an alluvial apron just beyond the mountain front. Had these models incorporated flexural subsidence in response to crustal thickening, the time required to fill the proximal portion of the basin and later remobilize these deposits would have been even greater. We suggest that a similar mechanism may account for the apparent delay between uplift of the Tibetan Plateau ($\sim 14+$ Ma) and the onset of rapid sedimentation in the northern Indian Ocean (~ 12 Ma).

Models based on a tectonic and stratigraphic reconstruction of the Zagros fold belt also show a time lag between the peak tectonic uplift rate and the peak sediment delivery rate. This represents the time scale for adjustment by the fluvial system, and is a function of rock resistance, the width of the region subject to uplift and erosion, and, assuming a nonlinear dependence of fluvial erosion upon channel gradient, of uplift rate. The dependence upon width implies that, all else being equal, narrower uplifts will produce a more punctuated sedimentary response than wider ones. The dependence of response time upon the degree of nonlinearity in the governing fluvial erosion equation underscores the need for better constraints on the long-term controls on bedrock stream incision.

Model erodibility parameters were calibrated by com-

© 1996 Blackwell Science Ltd,

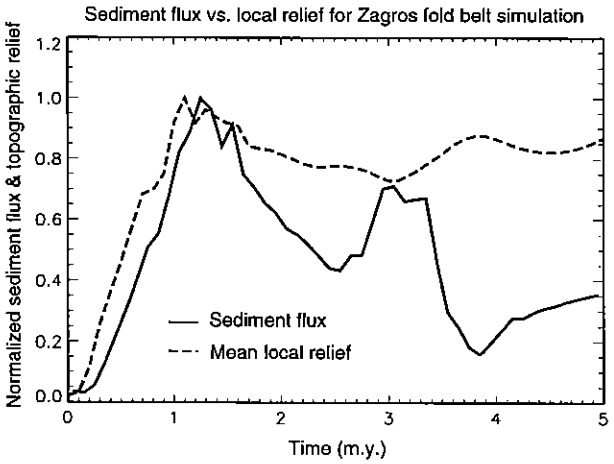

Fig. 16. Comparison of sediment flux versus mean local relief through time for the Zagros fold belt simulation pictured in Fig. 9. Mean local relief represents the average elevation difference between points spaced 20 km apart.

paring predicted topographic relief with the topographic relief observed in the Central Zagros Mountains, assuming a 10-fold erodibility contrast between weak and resistant lithologies. For a 40-km-wide fold belt, these values imply geomorphic response times on the order of 0.1–0.15 Myr for erodible lithologies and 3–4 Myr for resistant ones. Insofar as relief is likely to be more strongly influenced by the more resistant rocks, the latter value is more meaningful. Though this number is admittedly rather loosely constrained, it does suggest a geomorphic response time that is within the same order of magnitude as typical observed recurrence intervals between episodes of thrust activity in orogens.

On the other hand, model results also highlight the potential for significant natural variations in both geomorphic response time and in sediment supply rate, due to variations in rock resistance. Models based on the Zagros fold belt show significant sediment flux variations through time as lithologies of varying resistance to erosion are progressively exhumed. Such variations arise because a change in bedrock lithology corresponds to a change in the equilibrium longitudinal stream profile. As each new lithology is exhumed, a period of either accelerated or retarded stream downcutting occurs while streams readjust their longitudinal profiles. The significance of such lithologically produced sediment-flux variations depends in part upon the degree of lateral (as opposed to vertical) lithological homogeneity. If there is significant lateral heterogeneity (for example resulting from intense deformation), juxtaposition of multiple lithologies will tend to dampen any lithological influences on sediment supply. On the other hand, in cases where near-horizontal strata are subject to block-style uplift or broad upwarping, there exists the potential for a significant lithological control on sediment flux.

Model results also illustrate how stream capture and drainage diversion in response to folding or thrusting can lead to significant shifts in the location and magnitude of sediment source points. The scale of such depocentre shifts depends on the lateral extent of the structures involved, which for modern fold and thrust belts means tens to possibly hundreds of kilometres.

Finally, these models illustrate that when transverse drainage is completely cut off by a rising thrust, the temporary trapping of sediment within an intermontane basin can produce a significant mismatch between tectonic events and the rate and timing of sediment delivery to the outer foreland basin. In one such scenario, most of the orogenic sediment accumulates in an intermontane basin until the outer basin-bounding thrust is penetrated by a headward-eroding stream. A major pulse of sediment follows as the basin sediments are excavated. The timing of such an event may have little or nothing to do with the timing of tectonic events in the source terrain.

ACKNOWLEDGEMENTS

This work was funded in part by NASA Earth Observing System Grant, no. NAGW-2686. G.T. is grateful for support in the form of a NASA Graduate Fellowship in Global Change Research, no. NGT-30122. Our thanks to Daesy Geographics Laboratory for help in obtaining the data used to construct the DEM, and to C. Paola, D. Burbank and R. Robinson for constructive and helpful reviews.

REFERENCES

Ahnert, F. (1970) Function relationships between denudation, relief, and uplift in large mid-latitude drainage basins. *Am. J. Sci.*, **268**, 243–263.

Bagnold, R. A. (1966) An approach to the sediment transport problem from general physics. *Prof. Pap. U.S. Geol. Surv.*, **422-I**.

Berberian, M. (1995) Master 'blind' thrust faults hidden under the Zagros folds: active basement tectonics and surface morphotectonics. *Tectonophysics*, **241**, 193–224.

Berberian, M. & King, G. C. P. (1981) Towards a paleogeography and tectonic evolution of Iran. *Can. J. Earth Sci.*, **18**, 210–265.

Bird, P. (1978) Finite element modeling of lithosphere deformation: the Zagros collisional orogeny. *Tectonophysics*, **50**, 307–336.

Bridge, J. S. & Dominic, D. D. (1984) Bed load grain velocities and sediment transport rates. *Water Res. Rsch.*, **20**, 476–490.

Burbank, D. W. & Raynolds, R. G. H. (1988) Stratigraphic keys to the timing of thrusting in terrestrial foreland basins: applications to the northwestern Himalaya. In *New Perspectives in Basin Analysis* (Ed. by K. L. Kleinspehn and C. Paola), pp. 331–351. Springer-Verlag, New York.

Burbank, D. W. & Verges, J. (1994) Reconstruction of topography and related depositional systems during active thrusting. *J. geophys. Res.*, **99**, 20,281–20,297.

Cant, D. J. (1989) Simple equations of sedimentation: applications to sequence stratigraphy. *Basin Res.*, **2**, 73–81.

Cant, D. J. & Stockmal, G. S. (1994) Some controls on sedimentary sequences in foreland basins: examples from the Alberta Basin. In: *Tectonic Controls and Signatures in*

Sedimentary Successions (Ed. by L. E. Frostick and R. J. Steel), *Spec. Publ. int. Ass. Sediment.*, **20**, 49–65.

CARSON, M. A. & KIRKBY, M. J. (1972) *Hillslope Form and Process*. Cambridge University Press, New York.

CARSON, M. A. & PELTY, D. J. (1970) The existence of threshold hillslopes in the denudation of the landscape. *Trans. Inst. of Br. Geog.*, **49**, 71–95.

CHRISTIE-BLICK, N. (1991) Onlap, offlap, and the origin of unconformity-bounded depositional sequences. *Mar. Geol.*, **97**, 35–56.

COLEMAN, M. & HODGES, K. (1995) Evidence for Tibetan plateau uplift before 14 Myr ago from a new minimum age for east-west extension. *Nature*, **374**, 49–52.

COLMAN-SADD, S. P. (1978) Fold development in Zagros simply folded belt, southwest Iran. *Bull. Am. Ass. Petrol. Geol.*, **62**, 984–1003.

DEVLIN, W. J., RUDOLPH, K. W., SHAW, C. A. & EHMAN, K. D. (1993) The effect of tectonic and eustatic cycles on accommodation and sequence-stratigraphic framework in the Upper Cretaceous foreland basin of southwestern Wyoming. In: *Sequence Stratigraphy and Facies Associations* (Ed. by H. W. Posamentier *et al.*), *Spec. Publ. int. Ass. Sediment.*, **18**, 501–520.

FALCON, N. L. (1969) Problems of the relationship between surface structure and deep displacements illustrated by the Zagros range. In: *Time and Place in Orogeny* (Ed. by P. E. Kent, G. E. Satterhwaite and A. M. Spencer), *Geol. Soc. Spec. Publ.*, **3**, 9–22.

FALCON, N. L. (1974) Southern Iran: Zagros Mountains: In: *Mesozoic–Cenozoic Orogenic Belts, Data for Orogenic Studies* (Ed. by A. M. Spencer), *Geol. Soc. Spec. Publ.*, **4**, 199–211.

HACK, J. T. (1973a) Stream-profile analysis and stream-gradient index. *J. Res. U.S. Geol. Surv.*, **1**, 421–429.

HACK, J. T. (1973b) Drainage adjustment in the Appalachians. In: *Fluvial Geomorphology* (Ed. by M. Morisawa), pp. 51–69. SUNY Publications in Geomorphology, Binghampton, NY.

HAYNES, S. J. & MCQUILLAN, H. (1974) Evolution of the Zagros suture zone, southern Iran. *Bull. Geol. Soc. Am.*, **85**, 739–744.

HELLER, P. L., BURNS, B. A. & MARZO, M. (1993) Stratigraphic solution sets for determining the roles of sediment supply, subsidence, and sea level on transgressions and regressions. *Geology*, **21**, 747–750.

HOWARD, A. D. (1980) Thresholds in river regimes. In: *Thresholds in Geomorphology* (Ed. by D. R. Coates and J. D. Vitek), pp. 227–258. Allen and Unwin, Boston, MA.

HOWARD, A. D. (1987) Modelling fluvial systems: rock-, gravel- and sand- bed channels, In: *River Channels* (Ed. by K. Richards), pp. 69–94. Basil Blackwell, New York.

HOWARD, A. D. (1994) A detachment-limited model of drainage basin evolution. *Water Resour. Res.*, **30**, 2261–2285.

HOWARD, A. D., DIETRICH, W. E. & SEIDL, M. A. (1994) Modeling fluvial erosion on regional to continental scales. *J. geophys. Res.*, **99**, 13,971–13,986.

HOWARD, A. D. & KERBY, G. (1983) Channel changes in badlands. *Bull. Geol. Soc. Am.*, **94**, 739–752.

JAMES, G. A. & WYND, J. G. (1965) Stratigraphic nomenclature of Iranian Oil Consortium Agreement Area. *Bull. Am. Ass. Petrol. Geol.*, **49**, 2182–2245.

JERVEY, M. T. (1992) Siliciclastic sequence development in foreland basins, with examples from the Western Canada Foreland Basin. In: *Foreland Basins and Fold Belts* (Ed. by R. W. Macqueen and D. A. Leckie), *Mem. Am. Ass. Pet. Geol.*, **55**, 47–80.

JOLLEY, E. J., TURNER, P., WILLIAMS, G. D., HARTLEY, A. J. & FLINT, S. (1990) Sedimentological response of an alluvial system to Neogene thrust tectonics. *J. Geol. Soc. Lond.*, **147**, 769–784.

JORDAN, T. E. & FLEMINGS, P. B. (1991) Large-scale stratigraphic architecture, eustatic variation, and unsteady tectonism: a theoretical evaluation. *J. geophys. Res.*, **96**, 6681–6699.

KENDALL, C. G. ST. C. & LERCHE, I. (1988) The rise and fall of eustasy. In: *Sea Level Changes: An Integrated Approach* (Ed. by C. K. Wilgus, B. S. Hastings, C. G. St. C. Kendall, H. W. Posamentier, C. A. Ross & J. C. Van Wagoner), *Spec. Pub. SEPM*, **42**, 3–17.

KOOI, H. & BEAUMONT, C. (1996) Large-scale geomorphology: classical concepts reconciled and integrated with contemporary ideas via a surface processes model. *J. geophys. Res.*, **101**, 3361–3386.

MANN, C. D. & VITA-FINZI, C. (1988) Holocene serial folding in the Zagros. In: *Gondwana and Tethys* (Ed. by M. Audley-Charles & A. Hallam), *Spec. Publ. Geol. Soc.*, **37**, 51–59.

MARTINSEN, O. J., MARTINSEN, R. S. & STEIDTMANN, J. R. (1993) Mesaverde Group (Upper Cretaceous), southeastern Wyoming: allostratigraphy versus sequence stratigraphy in a tectonically active area. *Bull. Am. Ass. Pet. Geol.*, **77**, 1351–1373.

MILLIMAN, J. D. & SYVITSKI, J. P. M. (1992) Geomorphic/tectonic control of sediment discharge to the ocean: the importance of small mountainous rivers. *J. Geol.*, **100**, 525–544.

MOON, B. P. & SELBY, M. J. (1983) Rock mass strength and scarp forms in southern Africa. *Geogr. Annaler*, **65**, 135–145.

OBERLANDER, T. M. (1965) *The Zagros Streams*. Syracuse University Geographical Series, No. 1.

OBERLANDER, T. M. (1985) Origin of drainage transverse to structures in orogens. In: *Tectonic Geomorphology, Proceedings of the 15th Annual Binghampton Geomorphological Symposium* (Ed. by M. Morisawa & J. T. Hack), pp. 155–182. Allen and Unwin.

POSAMENTIER, H. W. & ALLEN, G. P. (1993a) Variability of the sequence stratigraphic model: effects of local basin factors. *Sediment. Geol.*, **86**, 91–109.

POSAMENTIER, H. W. & ALLEN, G. P. (1993b) Siliciclastic sequence stratigraphic patterns in foreland ramp-type basins. *Geology*, **21**, 455–458.

POSAMENTIER, H. W., JERVEY, M. T. & VAIL, P. R. (1988) Eustatic controls on clastic deposition I—conceptual framework. In: *Sea Level Changes: An Integrated Approach* (Ed. by C. K. Wilgus, B. S. Hastings, C. G. St. C. Kendall, H. W. Posamentier, C. A. Ross & J. C. Van Wagoner), *Spec. Pub. SEPM*, **42**, 109–124.

POSAMENTIER, H. W. & VAIL, P. R. (1988) Eustatic controls on clastic deposition II—sequence and systems track models. In: *Sea Level Changes: An Integrated Approach* (Ed. by C. K. Wilgus, B. S. Hastings, C. G. St. C. Kendall, H. W. Posamentier, C. A. Ross & J. C. Van Wagoner), *Spec. Pub. SEPM*, **42**, 124–154.

REA, D. K. (1992) Delivery of Himalayan sediment to the northern Indian Ocean and its relation to global climate, sea level, uplift, and seawater strontium. In: *Synthesis of Results from Scientific Drilling in the Indian Ocean* (Ed. by R. A. Duncan *et al.*), *Am. Geophys. Un. Monograph*, **70**, 387–402.

ROCKWELL, T. K., KELLER, E. A. & DEMBROFF, G. R. (1988) Quaternary rate of folding of the Ventura Avenue anticline,

western Transverse Ranges, southern California. *Bull. Geol. Soc. Am.*, **100**, 850–858.

SCHLAGER, W. (1993) Accommodation and supply—a dual control on stratigraphic sequences. *Sediment. Geol.*, **86**, 111–136.

SCHUMM, S. A. (1963) The disparity between present rates of denudation and orogeny. *Prof. Pap. U.S. Geol. Surv.*, **454-H**.

SCHUMM, S. A. & REA, D. K. (1995) Sediment yield from disturbed earth systems. *Geology*, **23**, 391–394.

SEIDL, M. A. & DIETRICH, W. E. (1992) The problem of channel erosion into bedrock. *Catena Suppl.*, **23**, 101–124.

SEIDL, M. A., DIETRICH, W. E. & KIRCHNER, J. W. (1994) Longitudinal profile development into bedrock: an analysis of Hawaiian channels. *J. Geol.*, **102**, 457–474.

SHANLEY, K. W. & MCCABE, P. J. (1994) Perspectives on the sequence stratigraphy of continental strata. *Bull. AAPG*, **78**, 544–568.

SLINGERLAND, R. L., HARBAUGH, J. W. & FURLONG, K. P. (1993) *Simulating Clastic Sedimentary Basins*. Prentice-Hall, New York.

SLINGERLAND, R. L. & ZHANG, F. (1991) High frequency sequence boundaries in the Price River Formation, Book Cliffs, Utah: A record of sea level or climate? *Geol. Soc. Am. Absts. with Progam*, **24**, 77.

STECKLER, M. S. & OMAR, G. I. (1994) Controls on erosional retreat of the uplifted rift flanks at the Gulf of Suez and northern Red Sea. *J. geophys. Res.*, **99**, 12,143–12,173.

STECKLER, M. S., REYNOLDS, D. J., COAKLEY, B. J., SWIFT, B. A. & JARRARD, R. (1993) Modelling passive margin sequence stratigraphy. In: *Sequence Stratigraphy and Facies Associations* (Ed. by H. W. Posamentier *et al.*), *Spec. Publ. int. Ass. Sediment.*, **18**, 19–41.

SUMMERFIELD, M. A. & HULTON, N. J. (1994) Natural controls of fluvial denudation rates in major world drainage basins. *J. geophys. Res.*, **99**, 13,871–13,883.

TALLING, P. J., LAWTON, T. F., BURBANK, D. W. & HOBBS, R. S. (1995) Evolution of latest Cretaceous-Eocene nonmarine deposystems in the Axhandle piggyback basin of central Utah. *Bull. Geol. Soc. Am.*, **107**, 297–315.

TUCKER, G. E. (1996) *Modelling the large-scale interaction of climate, tectonics, and topography*. PhD dissertation, Pennsylvania State University, University Park, PA.

TUCKER, G. E. & SLINGERLAND, R. L. (1994) Erosional dynamics, flexural isostasy, and long-lived escarpments: a numerical modeling study. *J. geophys. Res.*, **99**, 12,229–12,243.

WILLGOOSE, G. R., BRAS, R. L. & RODRIGUEZ-ITURBE, I. (1991) A physically based coupled network growth and hillslope evolution model. *Water Res. Rsch.*, **27**, 1671–1684.

WILLIAMS, G. D. & DOBB, A. (1993) *Tectonics and Seismic Sequence Stratigraphy, Geol. Soc. Lond. spec. publ.*, **71**.

YALIN, M. S. (1977) *Mechanics of Sediment Transport*, 2nd edn. Pargamon Press, New York.

YALIN, M. S. (1992) *River Mechanics*. Pergamon Press, New York.

Manuscript received 16 June 1995; revision accepted 9 November 1996.